Development 139, 2321-2329 (2012) doi:10.1242/dev.076406

Regulation of neuronal differentiation at the neurogenic wavefront

Pau Formosa-Jordan[1,2], Marta Ibañes[1,*], Saúl Ares[2,3,4,*,‡] and José María Frade[5,*,‡]

SUMMARY

Signaling mediated by the Delta/Notch system controls the process of lateral inhibition, known to regulate neurogenesis in metazoans. Lateral inhibition takes place in equivalence groups formed by cells having equal capacity to differentiate, and it results in the singling out of precursors, which subsequently become neurons. During normal development, areas of active neurogenesis spread through non-neurogenic regions in response to specific morphogens, giving rise to neurogenic wavefronts. Close contact of these wavefronts with non-neurogenic cells is expected to affect lateral inhibition. Therefore, a mechanism should exist in these regions to prevent disturbances of the lateral inhibitory process. Focusing on the developing chick retina, we show that *Dll1* is widely expressed by non-neurogenic precursors located at the periphery of this tissue, a region lacking *Notch1*, *lFng*, and differentiation-related gene expression. We investigated the role of this *Dll1* expression through mathematical modeling. Our analysis predicts that the absence of *Dll1* ahead of the neurogenic wavefront results in reduced robustness of the lateral inhibition process, often linked to enhanced neurogenesis and the presence of morphological alterations of the wavefront itself. These predictions are consistent with previous observations in the retina of mice in which *Dll1* is conditionally mutated. The predictive capacity of our mathematical model was confirmed further by mimicking published results on the perturbation of morphogenetic furrow progression in the eye imaginal disc of *Drosophila*. Altogether, we propose that Notch-independent Delta expression ahead of the neurogenic wavefront is required to avoid perturbations in lateral inhibition and wavefront progression, thus optimizing the neurogenic process.

KEY WORDS: Delta, Lateral inhibition, Mathematical modeling, Chick, *Drosophila*

INTRODUCTION

Notch/Delta signaling represents a major mechanism used by metazoans for cell fate decisions during development, in particular in the nervous system (Louvi and Artavanis-Tsakonas, 2006). The classical view, derived from early studies in *Drosophila*, states that neuronal precursors are formed in equivalence groups, in which cells have equal capacity to become neurons (Simpson and Carteret, 1990). Precursors expressing high levels of Delta induce Notch-dependent inhibitory signals in the neighboring cells. These inhibitory signals reduce the capacity of these cells to express proneural genes and *Delta* itself, preventing them from becoming neurons. In turn, the reduced capacity of the these inhibited precursors to trigger inhibitory signals facilitates the differentiation of the high Delta-expressing precursors. This mechanism has been referred to as 'lateral inhibition with feedback' (Collier et al., 1996).

Neuronal production is often initiated in restricted areas of the neurogenic epithelium, surrounded by non-neurogenic cells. As development proceeds, the neurogenic region expands, forming a wavefront at the boundary with the non-neurogenic tissue. The vertebrate retina represents a paradigmatic example. In this tissue, neurogenesis starts in its central region within a small cell cluster in response to specific signals (Stenkamp and Frey, 2003; Martinez-Morales et al., 2005), and then it gradually spreads to the periphery (Prada et al., 1991; Hu and Easter, 1999). Such spreading is largely dependent on the release of Sonic hedgehog (Shh) by the first neurons to be born in this tissue (Hu and Easter, 1999), the differentiated retinal ganglion cells (RGCs) (Neumann and Nuesslein-Volhard, 2000; Zhang and Yang, 2001; Stenkamp and Frey, 2003; Choy et al., 2010). This morphogen-dependent spreading of neurogenesis is reminiscent of the progression of the morphogenetic furrow (MF) in the *Drosophila* eye imaginal disc (Heberlein and Moses, 1995; Domínguez and Hafen, 1997).

The dynamic pattern of neurogenesis described above has important implications for the process of neuronal differentiation. Specifically, precursors located at the neurogenic wavefront are expected to receive fewer inhibitory signals than those inside the neurogenic region. This is because they are in direct contact with non-neurogenic precursors, which theoretically lack the capacity to trigger lateral inhibition. Therefore, the conditions at the wavefront are expected to have relevant consequences for the final pattern of neuronal differentiation. Although the importance of static boundary conditions at the borders of a pattern-forming tissue have received some theoretical notice (Honda et al., 1990; Collier et al., 1996; Murciano et al., 2002; Meir et al., 2002; Plahte, 2001), moving wavefronts of lateral inhibition have only recently come to attention (Owen, 2002; Plahte and Øyehaug, 2007; Pennington and Lubensky, 2010; O'Dea and King, 2011; Lubensky et al., 2011). These studies show how a neurogenic wavefront can sweep across a field of identical cells and leave behind a pattern of different cell types. However, the search for biological mechanisms used by metazoans to prevent disturbances in the pattern of neuronal differentiation associated with the existence of this wavefront remains open and represents a question of key importance.

[1]Department of Structure and Constituents of Matter, Faculty of Physics, University of Barcelona, E-08028 Barcelona, Spain. [2]Department of Biological Physics, Max-Planck Institute for the Physics of Complex Systems, D-01187 Dresden, Germany. [3]Logic of Genomic Systems Laboratory, Spanish National Biotechnology Centre CNB-CSIC, E-28049 Madrid, Spain. [4]Grupo Interdisciplinar de Sistemas Complejos (GISC). [5]Department of Molecular, Cellular and Developmental Neurobiology, Cajal Institute, IC-CSIC, E-28002 Madrid, Spain.

*Authors for correspondence (mibanes@ub.edu; saul.ares@csic.es; frade@cajal.csic.es)
‡These authors contributed equally to this work

Accepted 26 April 2012

Generalized *Delta* expression is often observed in prospective neural tissues and neurogenic boundary regions. For instance, in the early zebrafish embryo, strong *deltaD* expression delineates the whole developing retina a few hours before the initiation of neurogenesis in this tissue (Haddon et al., 1998; Kay et al., 2005). In both the avian and murine retina, *Delta-like 1* (*Dll1*) is expressed more peripherally than its homolog *Dll4*, being detected in a high proportion of mitotically active progenitor cells (Nelson and Reh, 2008; Rocha et al., 2009; Yang et al., 2009). In *Drosophila*, Delta (Dl) expression has been shown to precede achaete protein accumulation in microchaeta proneural stripes (Parks et al., 1997). Dl expression has also been described within eye imaginal discs of *Drosophila* on the surfaces of unpatterned cells ahead of the MF (Kooh et al., 1993; Baker and Zitron, 1995; Parks et al., 1995). As in other neural structures, generalized Dl expression ahead of the MF seems to be independent of canonical Notch signaling (Kunisch et al., 1994) as *hairy* (*h*), encoding a proneural gene repressor, and *extra macrochaetae* (*emc*), encoding an antagonist of the proneural gene products, are both expressed in this region (Brown et al., 1995). Delta expression in all these areas is often observed in most cells, suggesting that it is not a result of the lateral inhibitory process, but rather it represents a mechanism of mutual inhibition equally affecting all precursors (Goriely et al., 1991). Overall, these observations suggest that generalized *Delta* expression ahead of the neurogenic wavefront could be relevant in the process of lateral inhibition during neurogenesis.

Using the chick retina as a model system, we show that *Dll1* becomes expressed initially in its central region, prior to initiation of the neurogenic process. This pre-neurogenic expression of *Dll1* is maintained in the peripheral retina at later developmental stages, when active neurogenesis is not yet visualized in this area. From computer simulation results of a mathematical model for the initiation and morphogen-dependent spreading of the neurogenic process, which restricts the dynamics of lateral inhibition to the neurogenic region, we predict that the absence of Delta ahead of the neurogenic wavefront results in reduced robustness of the lateral inhibition process. Specifically, the absence of Delta is often linked to enhanced neurogenesis and, surprisingly, morphological alterations of the wavefront itself. These predictions could explain observations made by Rocha et al. (Rocha et al., 2009) in the retina of mice in which *Dll1* is conditionally mutated and Dll4-dependent lateral inhibition remains within the neurogenic region. Based on all this evidence, we suggest that generalized Delta expression ahead of the wavefront of neurogenesis is required for the avoidance of disturbances in lateral inhibition during the neuronal differentiation process. This might be extrapolated to other organisms and other neural tissues and could therefore be a general control mechanism of differentiation wavefronts.

MATERIALS AND METHODS

Chick embryos

Fertilized eggs from White-Leghorn hens were obtained from a local supplier (Granja Santa Isabel, Córdoba, Spain) and incubated at 38.5°C. The embryos were staged according to Hamburger and Hamilton (Hamburger and Hamilton, 1951). All experiments were performed in accordance with the European Union guidelines and they were previously approved by the CSIC animal ethics committee.

Reverse transcriptase-polymerase chain reaction (RT-PCR)

mRNA was extracted using the QuickPrep Micro mRNA purification kit (GE Healthcare), from which cDNA was prepared using the First-strand cDNA Synthesis Kit (GE Healthcare). PCR amplification was performed as described by Murciano et al. (Murciano et al., 2002). The following primers were employed: *Dll1* (bp 1764-1783, 2166-2185; accession number: U26590), *lFng* (bp 2319-2338, 2699-2718; accession number: U91849), *Atoh7* (bp 3-22, 460-479; accession number: U91849), *NeuroD1* (bp 323-342, 848-867; accession number: AF060885), *NeuroD4* (bp 470-489, 1087-1106; accession number: Y09597), *Ascl1* (bp 1005-1024, 1386-1405; accession number: NM_204412) and *Pou4f3* (bp 25-44, 486-505; accession number: NM_204759). The primers specific for *Notch1*, *Neurog2* and glyceraldehyde-3-phosphate dehydrogenase (*Gapdh*) have been described elsewhere (Murciano et al., 2002). *Gapdh* was amplified for 28 cycles, whereas the other genes were amplified for 29-35 cycles. Under these conditions, amplification was linear. No specific amplification was observed in the absence of reverse transcriptase.

Plasmids

DNA fragments from the coding sequences of chick *Atoh7* or *Pou4f3* were generated by RT-PCR (using the oligonucleotides described above) from mRNA extracts obtained from E5 chick retina (Quickprep Micro mRNA Purification Kit, GE Healthcare). These PCR fragments were then cloned in the pGEM-T Easy vector (Promega).

In situ hybridization

The digoxigenin-labeled antisense riboprobes for chick *Dll1*, *Notch1* and *lunatic Fringe* (*lFng*) were synthesized as described previously (Murciano et al., 2002; Cisneros et al., 2008). *Atoh7* and *Pou4f3* digoxigenin-labeled antisense riboprobes were obtained from linearized plasmid templates using T7 or Sp6 RNA polymerases as appropriate (Promega) following the manufacturer's instructions. In situ hybridization was performed as described previously (Murciano et al., 2002).

Mathematical model: equations

The temporal dynamics for the concentrations of the ligand l_i, signal s_i, readout r_i and morphogen m_i species in each cell i result from the difference between production of these molecules and their degradation and, in the case of the morphogen, also from its transport by diffusion. The dynamics are described by the following dimensionless equations:

$$\frac{dl_i}{dt} = v\left\{\frac{1}{1+bs_i^h} - l_i\right\}\Theta\left(m_i - m_c\right)\Theta\left(r_c - r_i\right) \quad (1)$$

$$\frac{ds_i}{dt} = \left\{\frac{k\left\langle l_i\right\rangle}{1+k\left\langle l_i\right\rangle} - s_i\right\}\Theta\left(m_i - m_c\right)\Theta\left(r_c - r_i\right) \quad (2)$$

$$\frac{dr_i}{dt} = v\left\{\frac{1}{1+bs_i^h} - r_i\right\}\Theta\left(m_i - m_c\right)\Theta\left(r_c - r_i\right) \quad (3)$$

$$\frac{dm_i}{dt} = u\left\{\Theta\left(r_i - r_c\right) + D\Delta_i m_i - m_i\right\}, \quad (4)$$

where the first term inside the large brackets corresponds to production and the last term to degradation. In these equations, v and u set the time scale of the ligand and morphogen dynamics, respectively; b controls the strength of ligand inhibition by the signal (the higher b, the stronger the inhibition); h is the Hill exponent for ligand repression cooperativity; k is related to the ligand-to-signal receptor affinity and gives the strength of Notch signaling (for higher k values, more signal up to saturation is triggered by ligand expression in neighboring cells); m_c is the morphogen concentration threshold over which a cell has lateral inhibition dynamics; and r_c is the readout threshold over which a cell is committed for differentiation, freezes its lateral inhibition and readout dynamics, and becomes a source of morphogen. Θ denotes the Heaviside step function, which is 1 when its argument is positive and 0 otherwise. $\langle l_i\rangle$ denotes the weighted sum of ligand concentration in the cells neighboring cell i and is given by Podgorski et al. (Podgorski et al., 2007):

$$\left\langle l_i\right\rangle = \frac{\sum_j \alpha_{ij} l_j}{\sum_j \alpha_{ij}}, \quad (5)$$

where the sum runs over all nearest neighbor cells j of cell i, and α_{ij} is the length of the boundary shared between cells i and j. $D\Delta_i m_i$ models the diffusion of the morphogen on an irregular lattice:

$$D\Delta_i m_i = \frac{D}{A_i}\sum_j \frac{\alpha_{ij}}{r_{ij}}\left(m_j - m_i\right), \quad (6)$$

with D being the non-dimensional diffusion rate of morphogen, A_i the area of cell i, and r_{ij} the distance between cell nodes i and j (Sukumar and Bolander, 2003).

We set the initial cells that act as morphogen sources to have the same dynamics (Eqns 1-3), except for the morphogen concentration, which reads $dm_i/dt=u\{1+D\Delta_i m_i-m_i\}$. Our results do not depend on the exact number or location of the initial morphogen source cells.

The equations for ligand (l_i), signal (s_i) and readout (r_i) consist of a production (synthesis) term minus a degradation term. The stochastic nature of gene expression arising from low copy number molecules has been included by extending the dynamics above for these three molecular species to the Langevin dynamics in the Itô interpretation (Gillespie, 2000; Gardiner, 2004):

$$\frac{dx_i}{dt} = PRODUCTION_i - DEGRADATION_i + \\ +\eta_{xi}(t)\sqrt{\left(PRODUCTION_i + |\,DEGRADATION_i\,|\right)/2V}\,, \quad (7)$$

where x denotes the molecular species (l, s or r), V is an effective volume of the cell and $\eta_{xi}(t)$ are stochastic variables of mean zero and variance $\langle \eta_{xi}(t)\ \eta_{x'j}(t')\rangle = 2\delta_{xx'}\,\delta_{ij}\,\delta(t-t')$ (i.e. uncorrelated Gaussian white noises), with $\delta_{xx'}$ being the Kronecker delta and $\delta(t-t')$ the delta functions.

We studied two distinct cases: wild type-like or Delta=1 case (supplementary material Fig. S1) in which the initial ligand concentration in all cells is high [$l_i(t=0)=1–0.1U_i$, where U_i is a uniform random number between 0 and 1]; and Delta=0 case (supplementary material Fig. S2) in which the initial concentration of ligand in all cells is low [$l_i(t=0)=0$]. In both cases, there is an initial low concentration of all the other species in all cells [$s_i=0$, $r_i=0$, $m_i=0$ at $t=0$].

Unless otherwise stated, we performed stochastic simulations with the following parameter values: $v=1$, $u=0.1$, $h=4$, $D=0.5625$, $m_c=0.001$, $r_c=0.5$, $V=2000$ in non-dimensional units. We choose the exponent $h=4$ to take into account in an effective way the nonlinearity introduced by intermediate processes not explicitly included in our phenomenological model. The ligand inhibition strength b and the signaling strength k are the control parameters of our study. Snapshots in figures and movies that show the pattern being formed have $b=10{,}000$ and $k=10$ unless otherwise stated. We checked that our results hold for a broad range of parameter values (supplementary material Figs S3-S13). Furthermore, for the full stochastic model we have repeated the parameter space characterization using values of the effective volume V between 100 and 5000, observing that our conclusions are robust to changes in the level of stochastic fluctuations.

Mathematical model: simulation details

Stochastic simulations were performed using a variation of Heun algorithm for the Itô interpretation (Carrillo et al., 2003) with a time step of 0.001. Gaussian random numbers were generated according to Toral and Chakrabarti (Toral and Chakrabarti, 1993). See supplementary material Fig. S1 for boundary conditions. See supplementary material Fig. S3 for the spatial arrangement and shape of cells.

Mathematical model: formal characterization of the growing neurogenic domain

We defined a neural density parameter ρ as $\rho=n_n^*/n_n$, with n_n^* being the number of neural cells and n_n the total number of cells within the neurogenic domain.

We defined a front morphology parameter Γ as $\Gamma=n_b^2/(12n_n)$, where n_b is the number of neurogenic cells in the border of the neurogenic domain. The pre-factor is defined such that $\Gamma\approx 1$ for a circular front morphology. $\Gamma\geq 1.5$ denotes fronts with a strong irregular morphology. Note that this parameter is related to the roundness shape descriptor (Russ, 2011).

We measured the effective radial velocity of the front v_f by fitting the time-evolution of the non-dimensional area of the neurogenic growing domain $a(t)$ to the expression $a(t)=\pi v_f^2 t^2$.

Estimation of the parameter region with stable pattern formation

We performed two theoretical analyses for the simplified version of the model, equivalent to that of Collier et al. (Collier et al., 1996) (Eqns 1 and 2 with $r_i<r_c$, $m_i>m_c$, $dr_i/dt=0$, $dm_i/dt=0$) for deterministic dynamics in a hexagonal lattice with periodic boundary conditions: a linear stability analysis of the homogeneous steady state (Collier et al., 1996) and an evaluation of the exact solutions with the periodicity of the lateral inhibition pattern (Formosa-Jordan and Ibañes, 2009). The results of these two analyses are plotted by solid and dashed lines, respectively, in all parameter space characterization figures. These analyses serve as a guide to the eye across parameter space and do not distinguish between the Delta=1 and Delta=0 cases because pattern propagation over a non-neurogenic tissue is not considered.

Drosophila morphogenetic furrow progression simulations

In our *Drosophila* MF progression simulations, we use the model described above (Eqns 1-7) and set the specificities of the MF as follows. We use periodic boundary conditions on the lateral boundaries of the field of cells, whereas the cells in the top and bottom rows have the morphogen concentration set to zero and no dynamics for the whole simulation. Cells in the third lowest row act as initial sources of morphogen. We simulated two different setups: one with initial high ligand and low signal concentration in all cells ($l_i=1\text{-}0.1U_i$, $s_i=0$) and uniform response (sensitivity) to morphogen levels ($m_c=0.001$), and another one with a patch of cells of variable size ten times more sensitive to the morphogen ($m_c=0.0001$), to reflect easier onset of Delta-Notch dynamics in h^-emc^- clones. We also performed simulations in which this patch of cells has normal sensitivity to the morphogen ($m_c=0.001$) but low initial ligand and signal expression ($l_i=0$, $s_i=0$). In all cases, all cells have no initial readout species r_i nor morphogen m_i. The velocity of the front v_f was fitted using the expression $a(t)=L\,v_f\,t$, where L is the non-dimensional length of the bottom boundary, which is 49 in all simulations.

RESULTS

Dll1 is expressed before the initiation of neurogenesis in the chick retina

Previous studies have shown generalized *Dll1* expression before retinal neuron differentiation (Haddon et al., 1998; Kay et al., 2005; Nelson and Reh, 2008; Rocha et al., 2009; Yang et al., 2009). We decided to investigate this issue by performing a systematic spatiotemporal analysis in the chick retina to evaluate the expression pattern of *Dll1* and other genes involved in the neurogenic process. With such an aim, mRNA was isolated from this tissue at different developmental stages ranging from Hamburger-Hamilton stage (HH) 15 to HH24, followed by RT-PCR with specific primers (Fig. 1A). *Dll1* was already detected at HH15, when neurogenesis is about to start (Prada et al., 1991). At HH15, *Notch1*, *lFng*, and the proneural genes *Neurog2*, *NeuroD1*, *NeuroD4* and *Atoh7* can hardly be detected (Fig. 1A). Together, this indicates that elevated *Dll1* expression in the chick retina can already be observed at a stage when neurogenesis is absent. *Dll1* expression is maintained throughout development following a pattern similar to that of the housekeeping gene *Gapdh*. By contrast, both *Notch1* and the aforementioned proneural genes steadily increase their expression levels at subsequent temporal stages, in accordance with the spreading of the neurogenic region towards the peripheral retina (Fig. 1A). *Acsl1* is first detected at HH20 (Fig. 1A), indicating that this proneural gene is expressed at relatively late stages of chick retinal development. High levels of

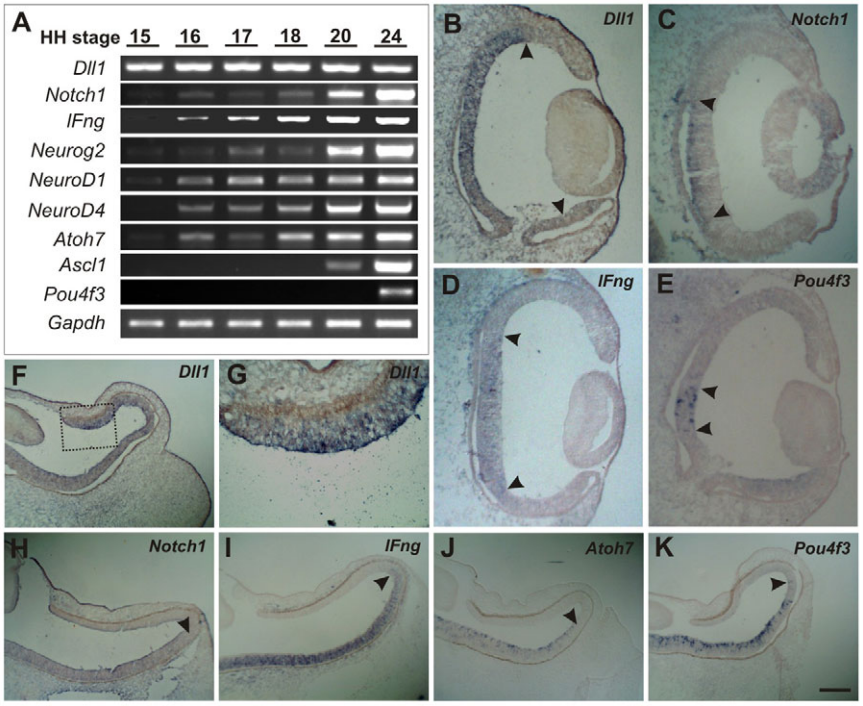

Fig. 1. Spatiotemporal expression pattern of genes involved in retinal neurogenesis. (**A**) RT-PCR analysis performed with specific primers in cDNAs obtained from chick retinas at the indicated developmental stages. (**B-K**) Cryostat sections from HH19 (B-E) or HH25 (F-K) chick retinas are shown. Panels illustrate representative in situ hybridizations with probes specific for the indicated transcripts (labeling in blue). Boxed area in F is shown at high magnification in G. Arrowheads indicate boundaries of expression. Scale bar: 60 μm (B-E), 150 μm (F-K).

Pou4f3 were first observed at HH24 (Fig. 1A), as expected from its late expression in a subpopulation of differentiated RGCs (Xiang et al., 1995).

The distinctive expression pattern of *Dll1* was confirmed by in situ hybridization. At stage HH19, *Dll1* expression was detected throughout most of the retinal neuroepithelium, reaching the peripheral retina (Fig. 1B). By contrast, we observed *Notch1* expression restricted to the central retina (Fig. 1C), where neurogenesis takes place as evidenced by the expression of the RGC-specific marker *Pou4f3* in just a few cells (Fig. 1E). This observation was confirmed at a later developmental stage (HH25), as previously shown by Nelson and Reh (Nelson and Reh, 2008). Thus, in situ hybridization with *Dll1*-specific probes demonstrated that this gene is readily expressed throughout the whole peripheral retina of the HH25 chick embryo (Fig. 1F,G). By contrast, *Notch1* expression is restricted to a more central region of the retina (Fig. 1H), where *Atoh7* expression is readily visible (Fig. 1J) and *Pou4f3* is heavily expressed (Fig. 1K), as expected from the strong signal observed for this gene by RT-PCR (Fig. 1A). Moreover, the expression of *Notch1* is correlated with an enrichment of transcripts specific for *lFng*, encoding a glycosyltransferase crucial for Notch signaling (Moloney et al., 2000) (Fig. 1D,I).

A model for lateral inhibition in the retina, controlled by a feedback-regulated diffusing morphogen

To gain insight into the role played by the distinctive *Dll1* expression described in the previous section, we used a mathematical model of the lateral inhibition process. We have modeled the developing retina as a two-dimensional tissue of irregularly shaped cells (Fig. 2A-C), where, for simplicity, we do not consider interkinetic nuclear movement (Murciano et al., 2002; Norden et al., 2009), cell death or cell division. Developmental events occurring after the advance of the initial neurogenic wave are out of the scope of our work. We model lateral inhibition using an extension of the model proposed by Lewis and co-workers (Collier et al., 1996). In this model, the expression of a ligand (*l*, Delta) in a cell is repressed by a signal (*s*, Notch) that is activated by the levels of ligand in the neighboring cells (Fig. 2B). We refer to *b* as the strength of Delta ligand inhibition by Notch, and *k* as the strength of Delta-driven Notch signaling activation by neighboring cells (see Fig. 2B). These two parameters control lateral inhibition dynamics and will be fundamental for further mathematical modeling (see below). To this basic model, we add the dynamics for a readout of differentiation species and a morphogen (see equations in Materials and methods).

The readout of differentiation could be identified with *Neurog2* and controls how close a cell is to starting differentiation. Because Notch inhibitory activity is downregulated just prior to RGC differentiation (Bellefroid et al., 1996; Nelson et al., 2006; Hämmerle et al., 2011), we set conditions such that the Delta-Notch lateral inhibition dynamics are stopped and the cell differentiates when its level of readout reaches an established threshold. The readout regulation is modeled replicating the ligand regulation.

The morphogen is set to diffuse from differentiated neurons and could be identified with Sonic hedgehog (Shh) or any other putative morphogen released from newly differentiated RGCs (Hufnagel et al., 2010). In this regard, Shh has been observed to diffuse from differentiated RGCs in chick (Zhang and Yang, 2001), mouse (Wang et al., 2005) and zebrafish (Neumann and Nuesslein-Volhard, 2000). In our model, the non-neurogenic cells ahead of the neurogenic wavefront that become exposed to high enough morphogen concentrations initiate lateral inhibition dynamics (Fig. 2B).

Altogether, the described dynamics can drive the following sequence of events (Fig. 2C). An initial morphogen source (Fig. 2C, cells with green layout at t=0) enables cells exposed to high levels of morphogen to enter into lateral inhibition dynamics (Fig. 2C, white cells at t=6). Driven by lateral inhibition, cells may reach high levels of readout and become differentiating RGCs (Fig. 2C, black cells at t=12). These differentiating cells then stop the ligand,

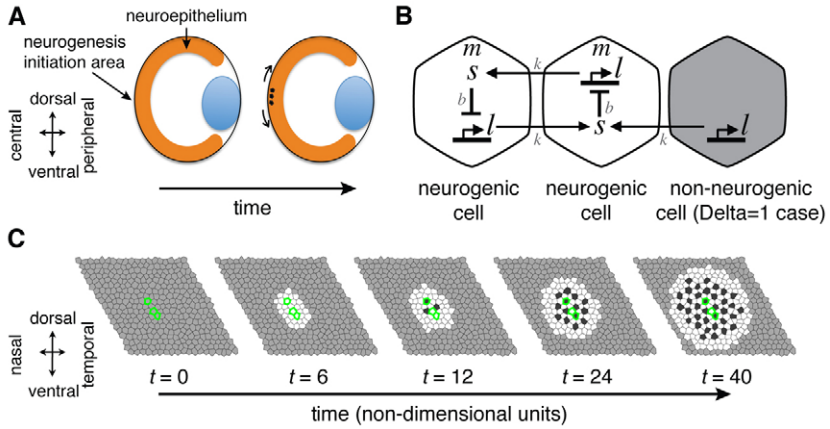

Fig. 2. A model for lateral inhibition in the chick retina. (**A**) Eye section cartoons before (left) and after (right) neurogenesis initiation. Small dots on the right panel represent differentiated neurons. Black arrows indicate front propagation. (**B**) Diagram illustrating the mathematical model. The presence of sufficient amount of Shh morphogen (*m*) makes cells neurogenic (left, center). These neurogenic cells are able to express proneural genes. Notch activation in these cells by Delta in neighboring cells triggers a Notch signal (*s*) inhibiting proneural gene expression and Delta ligand (*l*) expression. Parameters *b* and *k* denote strength of ligand inhibition and signaling activation, respectively. During neurogenic wavefront progression, neurogenic cells at the wavefront (center) are in direct contact with non-neurogenic cells ahead of it (right). In the wild type, non-neurogenic cells (right) are able to constitutively express Delta (Delta=1 case). This expression is lacking in the Delta=0 case discussed in the main text. (**C**) Snapshots of sequential time points of a wild-type simulation (Delta=1 case) of differentiation front propagation, showing only the central part of the simulated tissue. Light gray, non-neurogenic cells; white, neurogenic cells not committed to neural fate; dark gray, neurogenic cells committed to neural fate. The three cells with green contour in all panels denote the initial sources of morphogen. Parameters and details as indicated in Materials and methods.

signal and readout dynamics, and in turn become new sources of morphogen, which diffuses across the tissue. As a result, an expanding domain of active neurogenesis, where lateral inhibition takes place, can spread through non-neurogenic regions giving rise to neurogenic wavefronts (Fig. 2C, t=24 and t=40). Therefore, our model is able to account for a single neurogenic domain that grows regularly and homogeneously and leaves behind a lateral inhibition pattern of differentiated neurons, as occurs in wild-type chick retinas (Prada et al., 1991). A full characterization of the lateral inhibition pattern formed in terms of all model variables is shown in supplementary material Fig. S1.

Fig. 2C illustrates that active neurogenesis progression can be characterized in terms of the differentiation pattern being created, the shape of the neurogenic wavefront and the speed at which the wavefront advances through the non-neurogenic tissue (see Materials and methods). We defined the neural density ρ, i.e. the number of neural cells over the total number of cells within the neurogenic domain, to characterize the pattern of neurons being formed. For lateral inhibition patterns (Fig. 2C, t=40) the neural density is $\rho\approx1/3$. We defined the front morphology parameter Γ to characterize the shape of the wavefront. For a circular wavefront such as the one depicted in Fig. 2C, the front morphology parameter is $\Gamma\approx1$, whereas for irregular morphologies (see supplementary material Fig. S2 for an example) Γ is appreciably greater than 1. Lastly, we computed the speed v_f of wavefront progression from the expansion of the area of the neurogenic domain over time. We will use these three magnitudes to compare neurogenic progression under different conditions.

Notch-independent Dll1 expression ahead of the neurogenic boundary is crucial for the neurogenic process

To decipher the influence of Dll1 expression ahead of the neurogenic wavefront, we evaluated computationally two different situations. A first wild-type scenario (hereafter named Delta=1) which consists of generalized expression of Delta ligand in non-neurogenic regions (Fig. 2C; supplementary material Fig. S1), and a second mutant-like scenario (hereafter named Delta=0) in which non-neurogenic regions have no Delta expression (supplementary material Fig. S2).

Because quantitative values of all model parameters are unknown, we performed a search in parameter space to evaluate for which parameter values regular neurogenic progression leaving behind a lateral inhibition pattern occurs. We focused on those parameters controlling lateral inhibition dynamics: the strengths of Delta inhibition b and of signaling k.

We performed first a theoretical analysis of a simplified model to determine for which values of these two parameters stable pattern solutions can arise in a non-growing domain (see Materials and methods). Results are depicted with lines in Fig. 3. This analysis indicated that the patterned state (ρ=1/3) exists and is stable to small perturbations above the dashed line, whereas the homogeneous state with no pattern (ρ=0 or ρ=1) is stable to small perturbations below the solid line.

In the Delta=1 situation (Fig. 3A-C), a domain of active neurogenesis grows creating a lateral inhibition pattern ($\rho\approx1/3$), mostly above the dashed line. Moreover, in this region the neurogenic front advances with a regular circular shape as measured by the front morphology parameter ($\Gamma\approx1$; Fig. 3B) and with a moderate average front velocity ($v_f\approx0.15$ in non-dimensional units; Fig. 3C). Outside this region, two opposed situations are found (Fig. 3A,C): massive neurogenesis (neural density $\rho\approx1$) with very fast wavefront progression (front velocity $v_f>0.6$), and totally inhibited neural differentiation (neural density $\rho\approx0$) with no wavefront progression (front velocity $v_f\approx0$). Examples of the neurogenic domains that are formed for different parameter values, represented by points A, B, C and D in Fig. 3 are shown in Fig. 4 (left panels).

In the Delta=0 case (Fig. 3D-F), massive neurogenesis (i.e. neural density $\rho\approx1$) persisted for stronger signaling strength (k) compared with the Delta=1 situation (Fig. 3A,D, Fig. 4A).

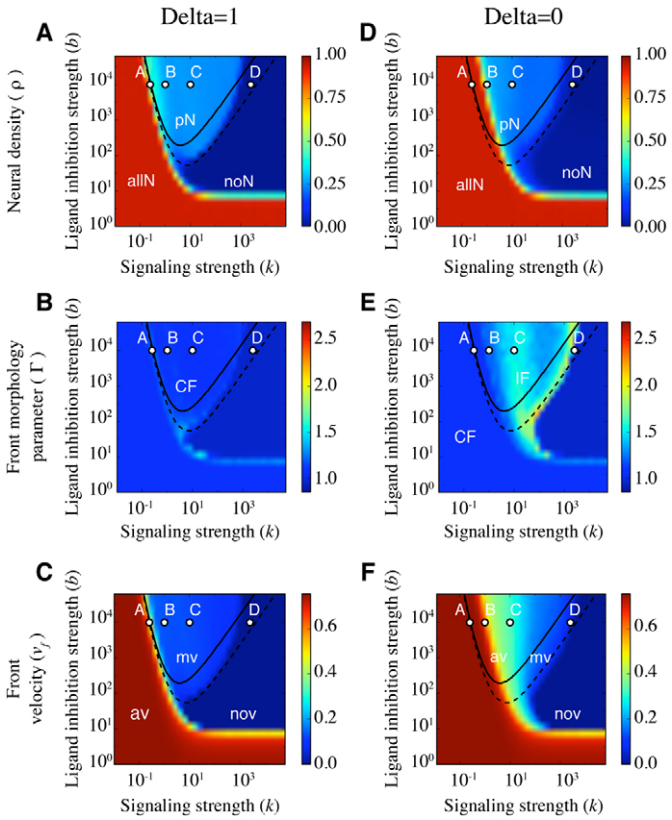

Fig. 3. Delta expression by non-neurogenic precursors promotes robustness of the lateral inhibition patterning process. (**A-F**) Parameter space characterization of the density of neurons ρ (A,D), the front morphology Γ (B,E) and the velocity of the front v_f (C,F) for Delta=1 (wild type-like, A-C) and Delta=0 (D-F) conditions. Each color band denotes the non-dimensional values of ρ, Γ and v_f, respectively. These values result from averages over ten different simulations of the full stochastic model (Eqns 1-7) at final simulation times. Lines stand for theoretical estimations of the pattern forming region (see Materials and methods). Letters A-D inside the diagrams denote different chosen representative points of the parameter space (patterns depicted in Fig. 4). The following abbreviations have been used to indicate different kinds of patterns: allN, massive neurogenesis; av, accelerated front velocity; CF, circular front; IF, irregular front; mv, intermediate front velocity; noN: no neurogenesis; nov: no front propagation; pN, common lateral inhibition pattern of neurogenesis. Parameter values are indicated in Materials and methods.

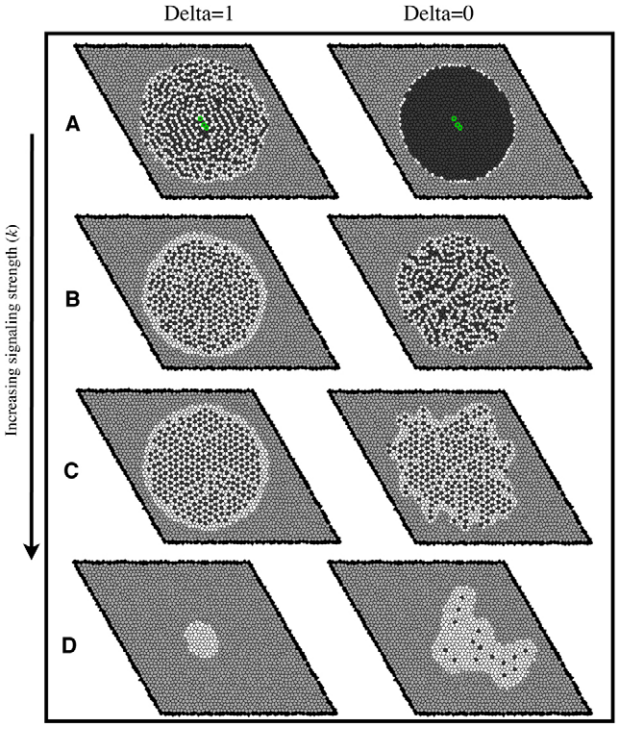

Fig. 4. Delta expression by non-neurogenic precursors promotes regular lateral inhibition patterning. (**A-D**) Snapshots of simulations of the neurogenic domain for Delta=1 (wild type-like, left column) and Delta=0 (right column) conditions. Different panels correspond to letters depicted in Fig. 3 with signaling strength values k=0.2511 (A), k=1 (B), k=10 (C), k=2511 (D); other parameters as specified in Materials and methods. Light gray, non-neurogenic cells; white, neurogenic cells not committed to neural fate; dark gray, neurogenic cells committed to neural fate. Patterns similar to those in C are typical for a wide region of parameter space. The same initial cell sources of morphogen were used in all panels but are only shown in A. Tissue boundary cells are depicted in black. Each snapshot corresponds to the final simulation time (see whole dynamics in supplementary material Movies 1-4).

Therefore, stronger signaling strength (k) is required in the absence of Delta in the non-neurogenic region to drive lateral inhibition patterning, which as a result arises in a reduced parameter space area (Fig. 3D, Fig. 4B).

Interestingly, our analysis also demonstrated that the neurogenic front acquires an irregular shape when Delta expression is absent from the non-neurogenic region (Fig. 4C). The irregular shape of the wavefront is characterized by high values of the front morphology parameter ($\Gamma \geq 1.5$; Fig. 3E). Front deformation occurs throughout most of the region in which the lateral inhibition pattern (neural density $\rho \approx 1/3$) arises. This result indicates that the presence of Delta throughout the non-neurogenic region can prevent the irregular spreading of neurons across the tissue as the neurogenic wavefront moves forward.

Moreover, our results show that the wavefront speeds up when Delta is absent from the non-neurogenic region, compared with the Delta=1 situation, especially for parameter values that enable the emergence of lateral inhibition patterns with moderate densities of neurons (Fig. 3F; supplementary material Movies 1-4).

Overall, our in silico experiments suggest a scenario in which Dll1 expression ahead of the neurogenic wavefront prevents neuronal overproduction and alterations in the morphology of the neurogenic wavefront, while controlling the correct timing of the neurogenic events.

Notch-independent Dl expression ahead of the neurogenic boundary is essential for regular morphogenetic furrow progression

To extend the implications of our model beyond retinal development in vertebrates, we focused on the developing *Drosophila* eye (Fig. 5A). In *Drosophila*, photoreceptor cells are born in response to the expression of the proneural gene *atonal* (*ato*), which locates within the morphogenetic furrow (MF) (Brown et al., 1995). The MF progresses throughout the eye imaginal disc driven by the diffusing morphogen Hh (Heberlein and Moses,

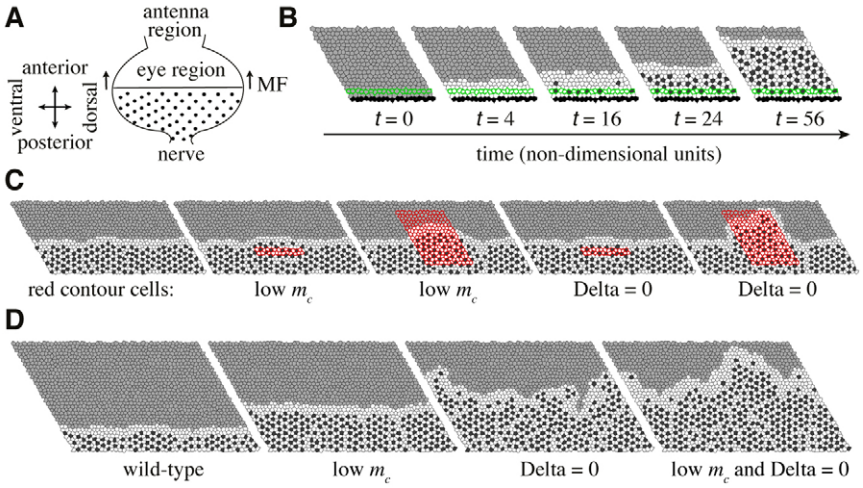

Fig. 5. Dynamics of wavefront progression in *Drosophila* eye disc. (**A**) Cartoon illustrating the eye region in *Drosophila* eye-antennal imaginal disc. Arrows denote morphogenetic furrow (MF) progression. Black dots, neural differentiated cells. (**B**) Snapshots of sequential time points of a wild-type simulation of MF progression. Light gray, non-neurogenic cells; white, neurogenic cells not committed to neural fate; dark gray, neurogenic cells committed to neural fate. Cells with green contour denote the initial sources of morphogen. Black cells on bottom rows denote boundary cells. (**C**) Snapshots of simulations of MF progression including cells in clones (red area) with different conditions, as indicated in the figure. Low m_c, ten times lower morphogen threshold (i.e. h^-/emc^-); Delta=0, non-neurogenic cells lack constitutive Delta expression. All snapshots correspond to the same time point; see supplementary material Movie 5 for dynamic progression. Simulations were run using the same seed for the random number generator. (**D**) Snapshots corresponding to the same time point of simulations of MF progression with different wavefront conditions, as indicated in the figure (see supplementary material Movie 6 for dynamics). The non-dimensional front velocity (from left to right) is v_f=0.18, 0.26, 0.34, 0.39. Parameters and details as indicated in Materials and methods. C and D show only the simulated area close to the MF. Whole simulated tissue is shown in supplementary material Movies 5 and 6.

1995; Domínguez and Hafen, 1997) (Fig. 5A). In this tissue, both Dl and Notch are expressed ahead of the MF (Fehon et al., 1991; Kooh et al., 1993) in the absence of proneural gene expression (Brown et al., 1995). Furthermore, *h* and *emc*, two regulatory genes known to respectively prevent proneural gene expression and function, are expressed just ahead of the MF (Brown et al., 1995), an area with potential neurogenic capacity owing to the indirect influence of MF-derived Hh (Greenwood and Struhl, 1999). This complex expression pattern is compatible with a scenario in which cells ahead of the MF express *Dl* in the absence of Delta/Notch dynamics, owing to the presence of h and emc. Null mutation of *h* and *emc* would facilitate lateral inhibition ahead of the MF (Brown et al., 1995).

In this context, we have developed a modification of our model characterized by the presence of a straight, linear neurogenic wavefront (compared with the circular wavefront in the modeling of the chick retina) that mimics neurogenesis at the MF in the eye imaginal disc of *Drosophila* (Fig. 5B; see Materials and methods). To test whether our model is compatible with empirical observations in *Drosophila*, we mimicked the experiments by Brown et al. (Brown et al., 1995). These authors showed that in mosaic eyes with large clones of cells lacking *emc* and *h* expression, the MF advances in a faster way over the clone. With narrow clones, no effect is observed. We modeled emc^-h^- clones with cells that have an increased sensitivity to Hh morphogen, triggering Delta/Notch lateral inhibition dynamics at a lower concentration of morphogen (Fig. 5C; supplementary material Movie 5). The left panel of Fig. 5C shows a snapshot of a simulation of our model for normal progression of the MF in the absence of an emc^-h^- clone. In the second panel, we see that a small clone has no effect on the progression of the furrow, as previously observed by Brown et al. (Brown et al., 1995). The third panel shows a snapshot of the faster advance of the differentiation front over a large emc^-h^- clone, in striking resemblance to observations in Brown et al. (Brown et al., 1995). This shows that our model can correctly reproduce perturbations of the conditions ahead of neurogenic fronts in situations beyond our initial study of neuronal differentiation in the vertebrate retina.

To compare this with our study of the chick retina, we simulated clones of low Delta ligand (Fig. 5C, fourth and fifth panels), obtaining results qualitatively similar to the case of increased neurogenic potential ahead of the MF (compare with second and third panel in Fig. 5C). An irregular wavefront seemed to arise additionally in the Delta=0 large clone (Fig. 5C, last panel). This is confirmed by simulations in which all cells ahead of the MF are either emc^-h^- or have absence of Delta ligand (Fig. 5D; supplementary material Movie 6). In comparison with the wild-type simulation (Fig. 5D, first panel), a faster progression occurs in each case (Fig. 5D, second and third panels) but irregular progression of the MF arises only in the absence of Delta ligand (Fig. 5D, third panel). When cells ahead the MF are emc^-h^- and, in addition, have no Delta ligand expression, MF progression is irregular too and slightly faster (Fig. 5D, fourth panel).

Despite the change in geometry (a linear wavefront in *Drosophila* vs a circular wavefront in the chick retina), these results are fully comparable to our study in the context of the chick retina. These results predict that Dl expression ahead of the neurogenic boundary is also essential for regular morphogenetic furrow progression in the *Drosophila* eye.

DISCUSSION

We have shown in the chick retina that *Dll1* is expressed in non-neurogenic regions ahead of the neurogenic wavefront in the absence of Delta/Notch dynamics. Our in silico experiments suggest that this *Dll1* expression can prevent both neuronal overproduction and alterations in the pattern of neuronal

differentiation, while controlling the correct timing of the neurogenic events. Our results are consistent with a model in which the absence of inhibition from neighboring non-neurogenic cells could lead to irregular accelerated neurogenesis in boundary neurogenic precursors and these irregularities would get amplified causing more distortion of the wavefront as neurogenesis continues to spread out. By contrast, Dll1 expression in non-neurogenic cells would prevent these distortions to occur. Interestingly, neuronal overproduction and alterations in the neurogenesis pattern can be observed in the developing retina of conditional knockout mice lacking *Dll1* expression, but maintaining lateral inhibition dynamics owing to *Dll4* expression within the neurogenic region (Rocha et al., 2009). Our results simulating the MF furrow in *Drosophila* also support the notion that Notch-independent Dl expression is crucial for maintaining the shape of the neurogenic wavefront. Unfortunately, the analysis of the influence of generalized *Dl* expression ahead of the MF in preventing neurogenic wavefront disturbances is hampered by its function as a proneural enhancer in this region, which results in the absence of retinal neurogenesis when mutated (Baker and Yu, 1997; Ligoxygakis et al., 1998).

The self-regulated mechanism for wavefront progression in the retina described in this study depends on the release of a diffusible morphogen that induces non-neurogenic cells to adopt a neurogenic fate. It has been proposed that the Shh-dependent mechanism does not take place in the mammalian retina (Wang et al., 2005), suggesting that morphogens other than Shh derived from newborn RGCs in mammals might participate in this process. Our model does not depend on the precise identity of the morphogen(s) involved in the process.

The mechanism described in this study could operate in other regions of the developing nervous system, also regulating neurogenic wavefronts. This could be the case for the chick caudal stem zone, a structure adjacent to the area showing active neurogenesis in the spinal cord. This caudal structure has been shown to express *Dll1* in a broad and uniform domain, prior to the establishment of lateral inhibition in the differentiating neuroepithelium (Akai et al., 2005). Nevertheless, unlike what is observed in the retina, neurogenic wavefront progression in the spinal cord seems to depend on an external source of retinoic acid, a morphogen released from mesodermal structures adjacent to the spinal cord (Diez del Corral et al., 2003).

Our results raise questions about the mechanism directing *Dll1* expression ahead of the neurogenic wavefront. In the chick caudal stem zone, generalized *Dll1* expression has been shown to depend on *Ascl2* (Akai et al., 2005), a proneural gene the murine homolog of which is absent from the retina (Mouse Genome Informatics accession ID: MGI:3499012) (Gray et al., 2004). In the mouse, *Ascl1* has been shown to induce *Dll1* expression when overexpressed in chick retinal explants (Nelson and Reh, 2008), but this effect is likely to be derived from the proneural nature of *Ascl1*, associated with its expression in Notch-active progenitors (Nelson et al., 2009). Therefore, the mechanism inducing *Dll1* expression in the HH15 chick retina, prior to *Ascl1* and *Notch1* detection, and in the most peripheral retina at later stages, where *Notch1* and *lFng* are absent, still remains unknown. The uncovering of such a mechanism will facilitate the design of experiments to test the predictions of our model further. One possible experiment to falsify our model would be the creation of knock-in mice in which *Dll1* promoter elements specific for Notch-independent *Dll1* expression are mutated. This genetic approach would inhibit Dll1 expression in the non-neurogenic region but not in neurogenic precursors undergoing lateral inhibition.

Together, our results show that the properties (pattern formed, shape and velocity) of progressing fronts of lateral inhibition, in our case neuronal differentiation, depend crucially on the conditions ahead of the differentiation front. Our observations regarding *Dll1* expression point to a mechanism for neurogenic front regulation in the retina, but as our study of the MF in the *Drosophila* eye shows, it could be an example of a more general developmental mechanism. Ligand expression in front of a lateral inhibition wavefront might act as a key regulator of differentiation processes.

Acknowledgements
We thank Ruth Diez del Corral, Juan R. Martínez-Morales, Caren Norden and Koichiro Uriu for critical reading of the manuscript; and Oriol Canela, José M. Sancho, Jaume Casademunt, Frank Jülicher, Luis G. Morelli, Peer Mumcu, Ernesto M. Nicola, Andrew C. Oates, and the Jülicher and Oates groups for discussion.

Funding
This study was supported by the Ministry of Science and Innovation (MICINN) [BFU2006-00805 and BFU2009-07671 to J.M.F., and MOSAICO to S.A.]; Fundación Lucha Contra la Ceguera (FundaLUCE) [J.M.F.]; Fondo de Investigaciones Sanitarias [FIS2006-11452-C03-01 and FIS2009-13360-C03-01 to P.F.-J. and M.I.]; and Generalitat de Catalunya [2005SGR00507 and 2009SGR14 to P.F.-J. and M.I.]. P.F.-J. acknowledges support from the FI program (Generalitat de Catalunya) and from a fellowship [FPU-AP2008-03325] supported by the Ministry of Education (2009-2011) and the Ministry of Education, Culture and Sports (2011-present). M.I. acknowledges funding from MICINN through the 'Ramón y Cajal' program. S.A. acknowledges a JAE-Doc contract [JAEDOC014, 2010 call] from the Spanish National Research Council (CSIC) program 'Junta para la Ampliación de Estudios' co-funded by European Social Fund (FSE).

Competing interests statement
The authors declare no competing financial interests.

Supplementary material
Supplementary material available online at
http://dev.biologists.org/lookup/suppl/doi:10.1242/dev.076406/-/DC1

References

Akai, J., Halley, P. A. and Storey, K. G. (2005). FGF-dependent Notch signaling maintains the spinal cord stem zone. *Genes Dev.* **19**, 2877-2887.
Baker, N. E. and Zitron, A. E. (1995). Drosophila eye development: Notch and Delta amplify a neurogenic pattern conferred on the morphogenetic furrow by scabrous. *Mech. Dev.* **49**, 173-189.
Baker, N. E. and Yu, S. Y. (1997). Proneural function of neurogenic genes in the developing Drosophila eye. *Curr. Biol.* **7**, 122-132.
Bellefroid, E. J., Bourguignon, C., Hollemann, T., Ma, Q., Anderson, D. J., Kintner, C. and Pieler, T. (1996). X-MyT1, a Xenopus C2HC-type zinc finger protein with a regulatory function in neuronal differentiation. *Cell* **87**, 1191-1202.
Brown, N. L., Sattler, C. A., Paddock, S. W. and Carroll, S. B. (1995). Hairy and Emc negatively regulate morphogenetic furrow progression in the Drosophila eye. *Cell* **80**, 879-887.
Carrillo, O., Ibañes, M., Garcia-Ojalvo, J., Casademunt, J. and Sancho, J. M. (2003). Intrinsic noise-induced phase transitions: Beyond the noise interpretation. *Phys. Rev. E* **67**, 46110.
Choy, S. W., Cheng, C. W., Lee, S. T., Li, V. W., Hui, M. N., Hui, C. C., Liu, D. and Cheng, S. H. (2010). A cascade of irx1a and irx2a controls shh expression during retinogenesis. *Dev. Dyn.* **239**, 3204-3214.
Cisneros, E., Latasa, M. J., García-Flores, M. and Frade, J. M. (2008). Instability of Notch1 and Delta1 mRNAs and reduced Notch activity in vertebrate neuroepithelial cells undergoing S-phase. *Mol. Cell. Neurosci.* **37**, 820-831.
Collier, J. R., Monk, N. A., Maini, P. K. and Lewis, J. H. (1996). Pattern formation by lateral inhibition with feedback: a mathematical model of Delta-Notch intercellular signalling. *J. Theor. Biol.* **183**, 429-446.
Diez del Corral, R., Olivera-Martinez, I., Goriely, A., Gale, E., Maden, M. and Storey, K. (2003). Opposing FGF and retinoid pathways control ventral neural pattern, neuronal differentiation, and segmentation during body axis extension. *Neuron* **40**, 65-79.

Domínguez, M. and Hafen, E. (1997). Hedgehog directly controls initiation and propagation of retinal differentiation in the Drosophila eye. *Genes Dev.* **11**, 3254-3264.
Fehon, R. G., Johansen, K., Rebay, I. and Artavanis-Tsakonas, S. (1991). Complex cellular and subcellular regulation of notch expression during embryonic and imaginal development of drosophila: implications for notch function. *J. Cell Biol.* **113**, 657-669.
Formosa-Jordan, P. and Ibañes, M. (2009). Diffusible ligand and lateral inhibition dynamics for pattern formation. *J. Stat. Mech.* **2009**, P03019.
Gardiner, C. W. (2004). *Handbook of stochastic methods for physics, chemistry and the natural sciences*. Berlin: Springer-Verlag.
Gillespie, D. T. (2000). The chemical Langevin equation. *J. Chem. Phys.* **113**, 297-306.
Goriely, A., Dumont, N., Dambly-Chaudière, C. and Ghysen, A. (1991). The determination of sense organs in Drosophila: effect of neurogenic mutations in the embryo. *Development* **113**, 1395-1404.
Gray, P. A., Fu, H., Luo, P., Zhao, Q., Yu, J., Ferrari, A., Tenzen, T., Yuk, D. I., Tsung, E. F., Cai, Z. et al. (2004). Mouse brain organization revealed through direct genome-scale TF expression analysis. *Science* **306**, 2255-2257.
Greenwood, S. and Struhl, G. (1999). Progression of the morphogenetic furrow in the Drosophila eye: the roles of Hedgehog, Decapentaplegic and the Raf pathway. *Development* **126**, 5795-5808.
Haddon, C., Smithers, L., Schneider-Maunoury, S., Coche, T., Henrique, D. and Lewis, J. (1998). Multiple *delta* genes and lateral inhibition in zebrafish primary neurogenesis. *Development* **125**, 359-370.
Hamburger, V. and Hamilton, H. L. (1951). A series of normal stages in the development of the chick embryo. *J. Morphol.* **88**, 49-92.
Hämmerle, B., Ulin, E., Guimera, J., Becker, W., Guillemot, F. and Tejedor, F. J. (2011). Transient expression of Mnb/Dyrk1a couples cell cycle exit and differentiation of neuronal precursors by inducing p27KIP1 expression and suppressing NOTCH signaling. *Development* **138**, 2543-2554.
Heberlein, U. and Moses, K. (1995). Mechanisms of Drosophila retinal morphogenesis: the virtues of being progressive. *Cell* **81**, 987-890.
Honda, H., Tanemura, M. and Yoshida, A. (1990). Estimation of neuroblast numbers in insect neurogenesis using the lateral inhibition hypothesis of cell differentiation. *Development* **110**, 1349-1352.
Hu, M. and Easter, S. S. (1999). Retinal neurogenesis: the formation of the initial central patch of postmitotic cells. *Dev. Biol.* **207**, 309-321.
Hufnagel, R. B., Le, T. T., Riesenberg, A. L. and Brown, N. L. (2010). Neurog2 controls the leading edge of neurogenesis in the mammalian retina. *Dev. Biol.* **340**, 490-503.
Kay, J. N., Link, B. A. and Baier, H. (2005). Staggered cell-intrinsic timing of ath5 expression underlies the wave of ganglion cell neurogenesis in the zebrafish retina. *Development* **132**, 2573-2585.
Kooh, P. J., Fehon, R. G. and Muskavitch, M. A. (1993). Implications of dynamic patterns of Delta and Notch expression for cellular interactions during Drosophila development. *Development* **117**, 493-507.
Kunisch, M., Haenlin, M. and Campos-Ortega, J. A. (1994). Lateral inhibition mediated by the Drosophila neurogenic gene delta is enhanced by proneural proteins. *Proc. Natl. Acad. Sci. USA* **91**, 10139-10143.
Ligoxygakis, P., Yu, S. Y., Delidakis, C. and Baker, N. E. (1998). A subset of Notch functions during Drosophila eye development require Su(H) and the E(spl) gene complex. *Development* **125**, 2893-2900.
Louvi, A. and Artavanis-Tsakonas, S. (2006). Notch signalling in vertebrate neural development. *Nat. Rev. Neurosci.* **7**, 93-102.
Lubensky, D. K., Pennington, M. W., Shraiman, B. I. and Baker, N. E. (2011). A dynamical model of ommatidial crystal formation. *Proc. Natl. Acad. Sci. USA* **108**, 11145-11150.
Martinez-Morales, J. R., Del Bene, F., Nica, G., Hammerschmidt, M., Bovolenta, P. and Wittbrodt, J. (2005). Differentiation of the vertebrate retina is coordinated by an FGF signaling center. *Dev. Cell* **8**, 565-574.
Meir, E., von Dassow, G., Munro, E. and Odell, G. M. (2002). Robustness, flexibility, and the role of lateral inhibition in the neurogenic network. *Curr. Biol.* **12**, 778-786.
Moloney, D. J., Panin, V. M., Johnston, S. H., Chen, J., Shao, L., Wilson, R., Wang, Y., Stanley, P., Irvine, K. D., Haltiwanger, R. S. and Vogt, T. F. (2000). Fringe is a glycosyltransferase that modifies Notch. *Nature* **406**, 369-375.
Murciano, A., Zamora, J., López-Sánchez, J. and Frade, J. M. (2002). Interkinetic nuclear movement may provide spatial clues to the regulation of neurogenesis. *Mol. Cell. Neurosci.* **21**, 285-300.
Nelson, B. R. and Reh, T. A. (2008). Relationship between Delta-like and proneural bHLH genes during chick retinal development. *Dev. Dyn.* **237**, 1565-1580.
Nelson, B. R., Gumuscu, B., Hartman, B. H. and Reh, T. A. (2006). Notch activity is downregulated just prior to retinal ganglion cell differentiation. *Dev. Neurosci.* **28**, 128-141.
Nelson, B. R., Hartman, B. H., Ray, C. A., Hayashi, T., Bermingham-McDonogh, O. and Reh, T. A. (2009). Acheate-scute like 1 (Ascl1) is required for normal delta-like (Dll) gene expression and Notch signaling during retinal development. *Dev. Dyn.* **238**, 2163-2178.
Neumann, C. J. and Nuesslein-Volhard, C. (2000). Patterning of the zebrafish retina by a wave of sonic hedgehog activity. *Science* **289**, 2137-2139.
Norden, C., Young, S., Link, B. A. and Harris, W. A. (2009). Actomyosin is the main driver of interkinetic nuclear migration in the retina. *Cell* **138**, 1195-1208.
O'Dea, R. D. and King, J. R. (2011). Multiscale analysis of pattern formation via intercellular signalling. *Math. Biosci.* **231**, 172-185.
Owen, M. R. (2002). Waves and propagation failure in discrete space models with nonlinear coupling and feedback. *Physica D* **173**, 59-76.
Parks, A. L., Turner, F. R. and Muskavitch, M. A. (1995). Relationships between complex Delta expression and the specification of retinal cell fates during Drosophila eye development. *Mech. Dev.* **50**, 201-216.
Parks, A. L., Huppert, S. S. and Muskavitch, M. A. (1997). The dynamics of neurogenic signaling underlying bristle development in Drosophila melanogaster. *Mech. Dev.* **63**, 61-74.
Pennington, M. W. and Lubensky, D. K. (2010). Switch and template pattern formation in a discrete reaction-diffusion system inspired by the Drosophila eye. *Eur. Phys. J. E* **33**, 129-148.
Plahte, E. (2001). Pattern formation in discrete cell lattices. *J. Math. Biol.* **43**, 411-445.
Plahte, E. and Øyehaug, L. (2007). Pattern-generating travelling waves in a discrete multicellular system with lateral inhibition. *Physica D* **226**, 117-128.
Podgorski, G. J., Bansal, M. and Flann, N. S. (2007). Regular mosaic pattern development: A study of the interplay between lateral inhibition, apoptosis and differential adhesion. *Theor. Biol. Med. Model.* **4**, 43.
Prada, C., Puga, J., Pérez-Méndez, L., López, R. and Ramírez, G. (1991). Spatial and Temporal Patterns of Neurogenesis in the Chick Retina. *Eur. J. Neurosci.* **3**, 559-569.
Rocha, S. F., Lopes, S. S., Gossler, A. and Henrique, D. (2009). Dll1 and Dll4 function sequentially in the retina and pV2 domain of the spinal cord to regulate neurogenesis and create cell diversity. *Dev. Biol.* **328**, 54-65.
Russ, J. C. (2011). *The Image Processing Handbook*. Boca Raton: CRC Press.
Simpson, P. and Carteret, C. (1990). Proneural clusters: equivalence groups in the epithelium of Drosophila. *Development* **110**, 927-932.
Stenkamp, D. L. and Frey, R. A. (2003). Extraretinal and retinal hedgehog signaling sequentially regulate retinal differentiation in zebrafish. *Dev. Biol.* **258**, 349-363.
Sukumar, N. and Bolander, J. E. (2003). Numerical computation of discrete differential operators on non-uniform grids. *CMES-Comp. Model. Eng.* **4**, 691-706.
Toral, R. and Chakrabarti, A. (1993). Generation of Gaussian distributed random numbers by using a numerical inversion method. *Comp. Phys. Commun.* **74**, 327.
Wang, Y., Dakubo, G. D., Thurig, S., Mazerolle, C. J. and Wallace, V. A. (2005). Retinal ganglion cell-derived sonic hedgehog locally controls proliferation and the timing of RGC development in the embryonic mouse retina. *Development* **132**, 5103-5113.
Xiang, M., Zhou, L., Macke, J. P., Yoshioka, T., Hendry, S. H., Eddy, R. L., Shows, T. B. and Nathans, J. (1995). The Brn-3 family of POU-domain factors: primary structure, binding specificity, and expression in subsets of retinal ganglion cells and somatosensory neurons. *J. Neurosci.* **15**, 4762-4785.
Yang, H. J., Silva, A. O., Koyano-Nakagawa, N. and McLoon, S. C. (2009). Progenitor cell maturation in the developing vertebrate retina. *Dev. Dyn.* **238**, 2823-2836.
Zhang, X. M. and Yang, X. J. (2001). Regulation of retinal ganglion cell production by Sonic hedgehog. *Development* **128**, 943-957.

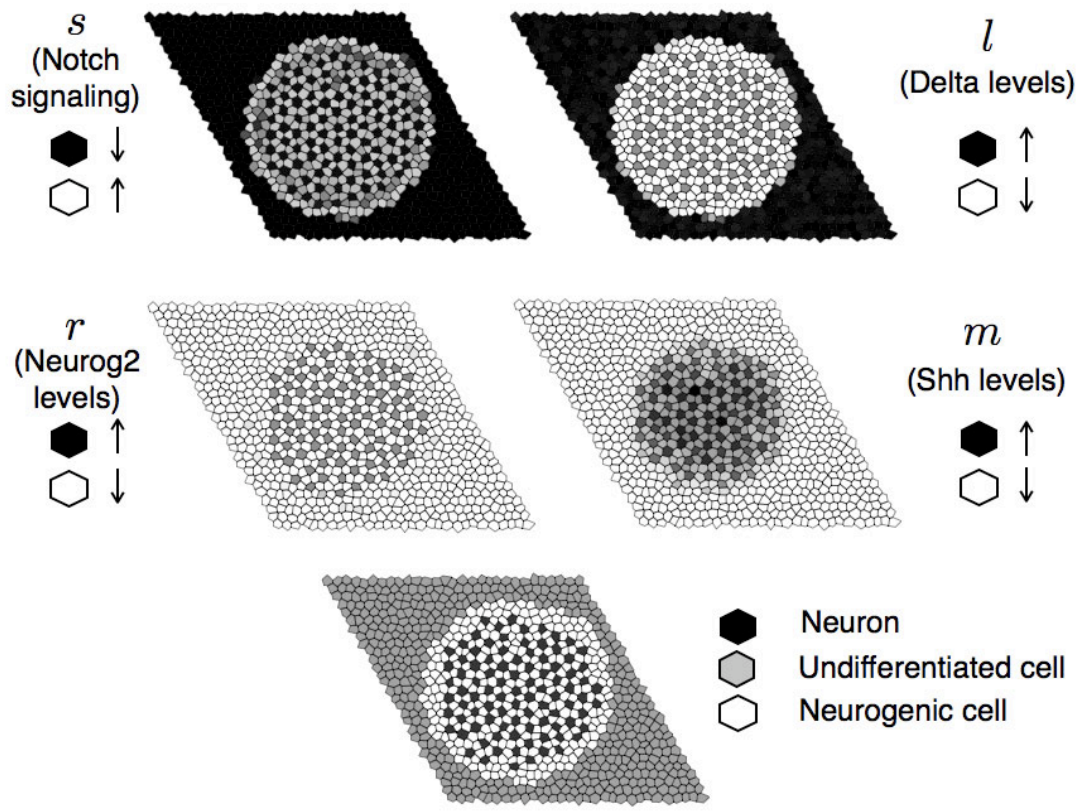

Fig. S1. Full single-cell state characterization of a neurogenic domain for Delta=1 condition. All panels correspond to the same neurogenic domain. Each panel depicts the level of a different state variable (which is indicated next to the snapshot). Grayscale codes for each variable are indicated in the figure. Note that Notch has opposite grayscale code. The bottom panel corresponds to the type of snapshot shown in Figs 2 and 4, depicting the differentiation state of cells. To facilitate single-cell resolution, we show only the central part of the overall tissue. The neurogenic domain corresponds to a stochastic simulation on an irregular array of 49×49 cells for k=10 and b=10,000 in Delta=1 conditions with a single central cell acting as first source of Shh. Other parameter values as in Materials and methods in the main text. Note that the oversimplified picture of intercellular signaling used here is an effective model and it does not intend to simulate in a quantitative way concentrations of actual molecular species. To avoid boundary effects, we stop our simulations when the first cells at a

distance of five cells from the simulation boundary enter into lateral inhibition dynamics. To avoid unnecessary long simulation runs, we also set a rule to stop simulations with extremely slow dynamics. The boundary condition for the morphogen m_i at the boundary of the simulated field of cells is set to zero morphogen concentration.

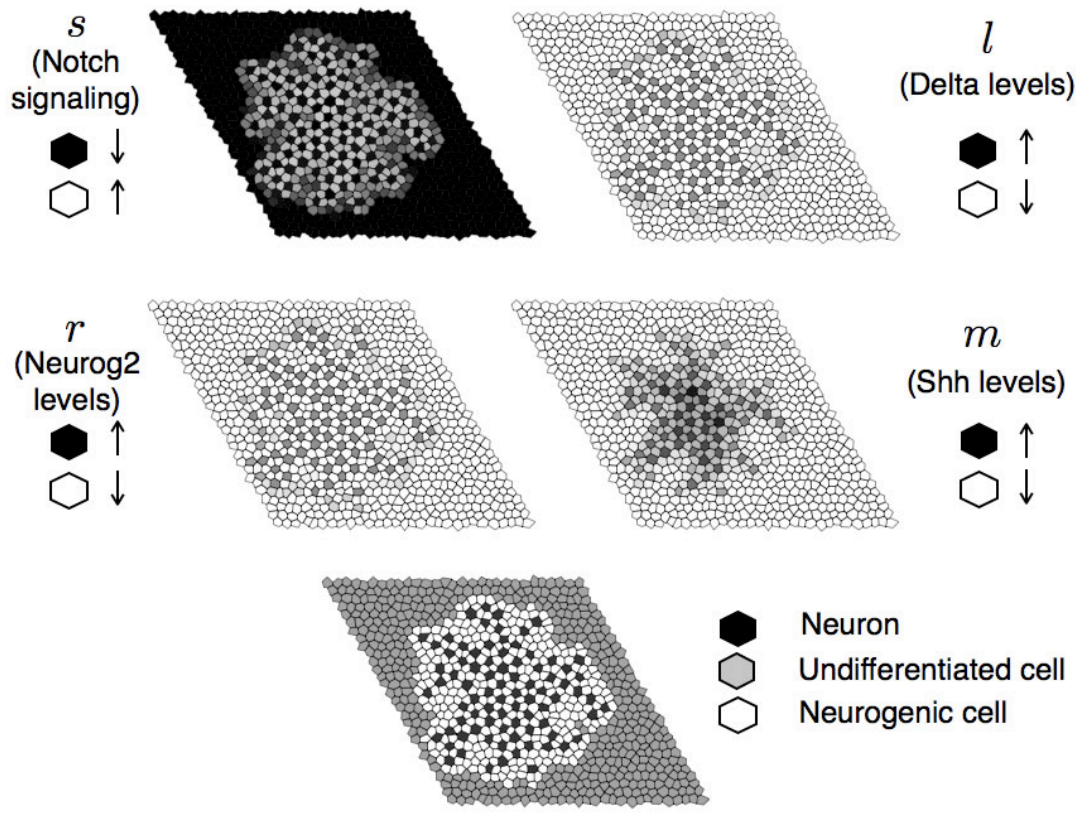

Fig. S2. Full single-cell state characterization of a neurogenic domain for Delta=0 condition. All panels correspond to the same neurogenic domain. Each panel depicts the level of a different state variable (which is indicated next to the snapshot). Grayscale codes for each variable are indicated in the figure. Note that Notch has opposite grayscale code. The bottom panel corresponds to the type of snapshot shown in Fig. 4, depicting the differentiation state of cells. To facilitate single-cell resolution, we show only the central part of the overall tissue. The neurogenic domain corresponds to a stochastic simulation on an irregular array of 49×49 cells for k=10 and b=10,000 in Delta=0 conditions with a single central cell acting as first source of Shh. Other parameter values as in Materials and methods in the main text.

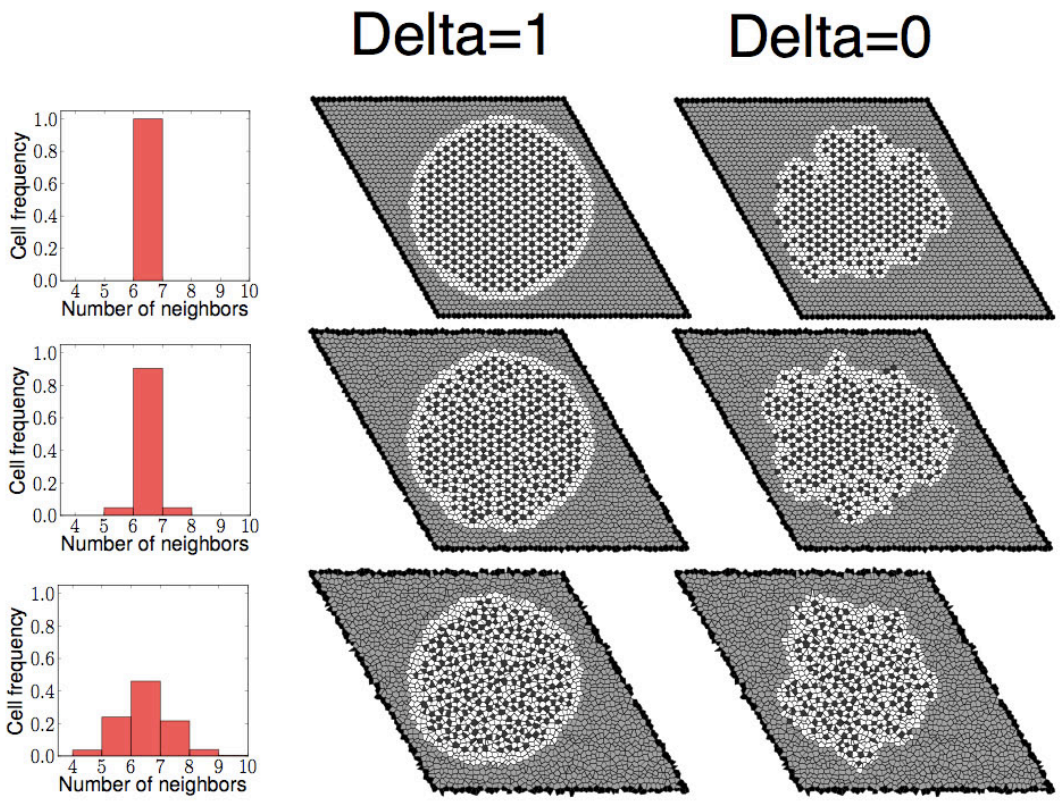

Fig. S3. The irregularity of the lattice does not alter the qualitative features of patterns. To construct the spatial layout of cells we generate an irregular distribution of points on a plane starting from a perfect triangular lattice and displacing the position **r** of each point to a new position **r′** given by $\mathbf{r}' = \mathbf{r} + \frac{\gamma}{\Lambda}\{(\upsilon_x - 0.5)\mathbf{x} + (\upsilon_y - 0.5)\mathbf{y}\}$, where Λ is the distance between first nearest neighbor nodes on the triangular lattice and υ_x and υ_y are random numbers drawn from an uniform distribution between 0 and 1. γ sets the magnitude of irregularity of the resulting lattice such that the resulting field is composed of equal perfectly hexagonal cells for $\gamma=0$, and irregularity increases with increasing γ. Unless otherwise stated, in this work we use lattices of 49×49 irregular cells with Λ=1 and γ=1.6. A Voronoi tessellation is created around these points using Mathematica's Computational Geometry Package (Wolfram Research, 2008, Mathematica, Version 7.0, Champaign, IL, USA). This figure shows the

characterization of the number of neighbors of each cell (left column) and of the emerging pattern for Delta=1 (middle column) and Delta=0 (right column) conditions for lattice irregularity parameters γ=0.67 (top row), γ=1.6 (middle row) and γ=2.67 (bottom row). Although for γ=0.67 all cells have six neighbors, cell side lengths (and, accordingly, the strength of the ligand-receptor interaction) are not regular. Hence, the hexagonal symmetry is lost and the instability of the front does not follow the hexagonal symmetry that one can observe in perfect hexagonal lattices (supplementary material Figs. S5, S9, S11-S13). Grayscale code as in last row of supplementary material Fig. S1. Patterns correspond to a stochastic simulation for k=10. All remaining parameters and conditions are as in supplementary material Fig. S1.

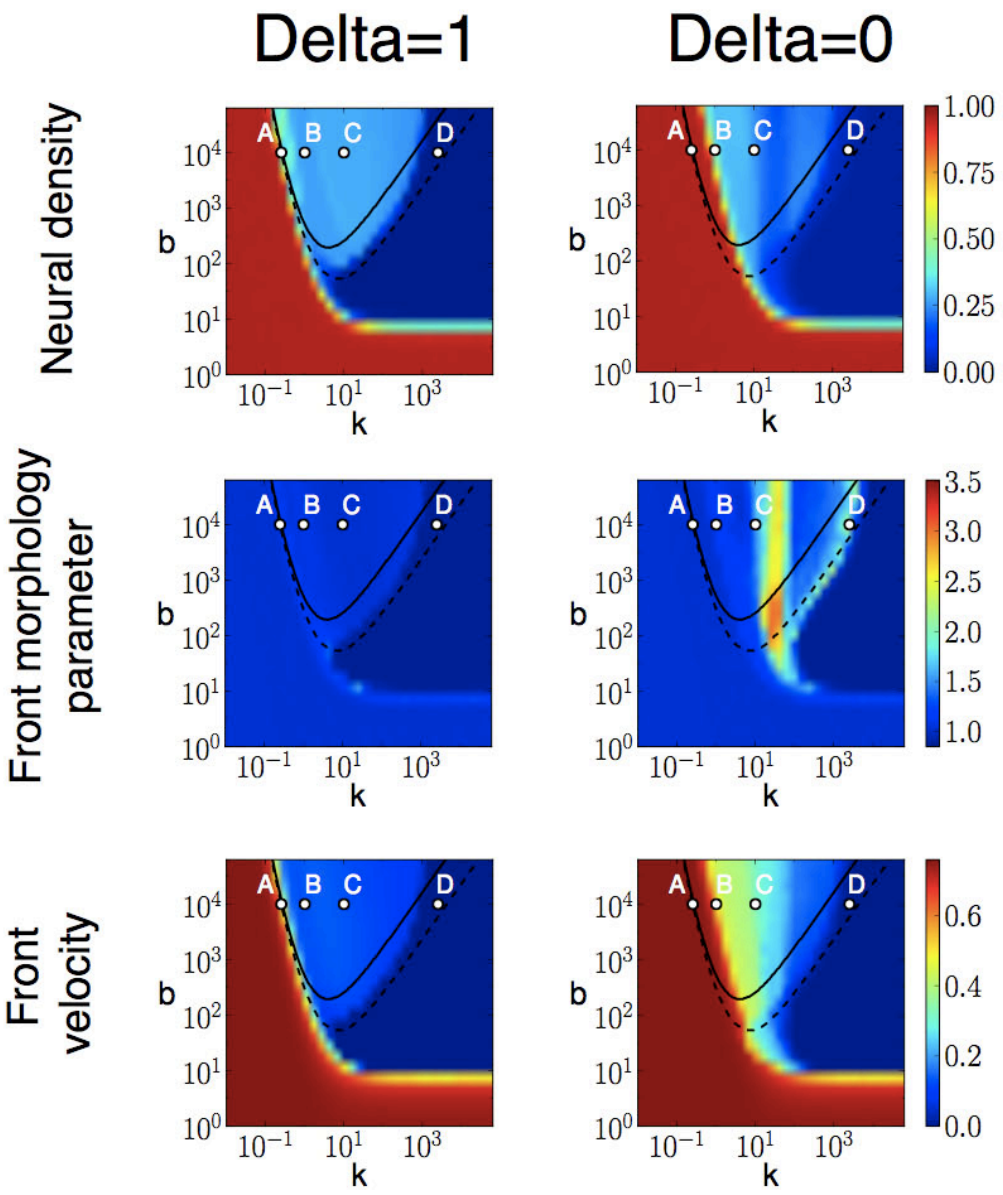

Fig. S4. Dynamics on hexagonal regular lattices show similar qualitative results. Parameter space characterization of ρ (first row), Γ (second row) and v_f (third row) for Delta=1 conditions (left column) and Delta=0 conditions (right column) as in Fig. 3 of the main text but on a regular hexagonal lattice and with a single central morphogen source. Results are averages over ten stochastic simulations. Letters inside the diagrams denote different chosen representative points of the parameter space (see supplementary material Fig. S5). All remaining parameters and conditions are as in Fig. 3 of the main text. Results are very similar to those in Fig. 3 of the main text, but differences in the

front morphology parameter between the Delta=1 and the Delta=0 scenario are accentuated here.

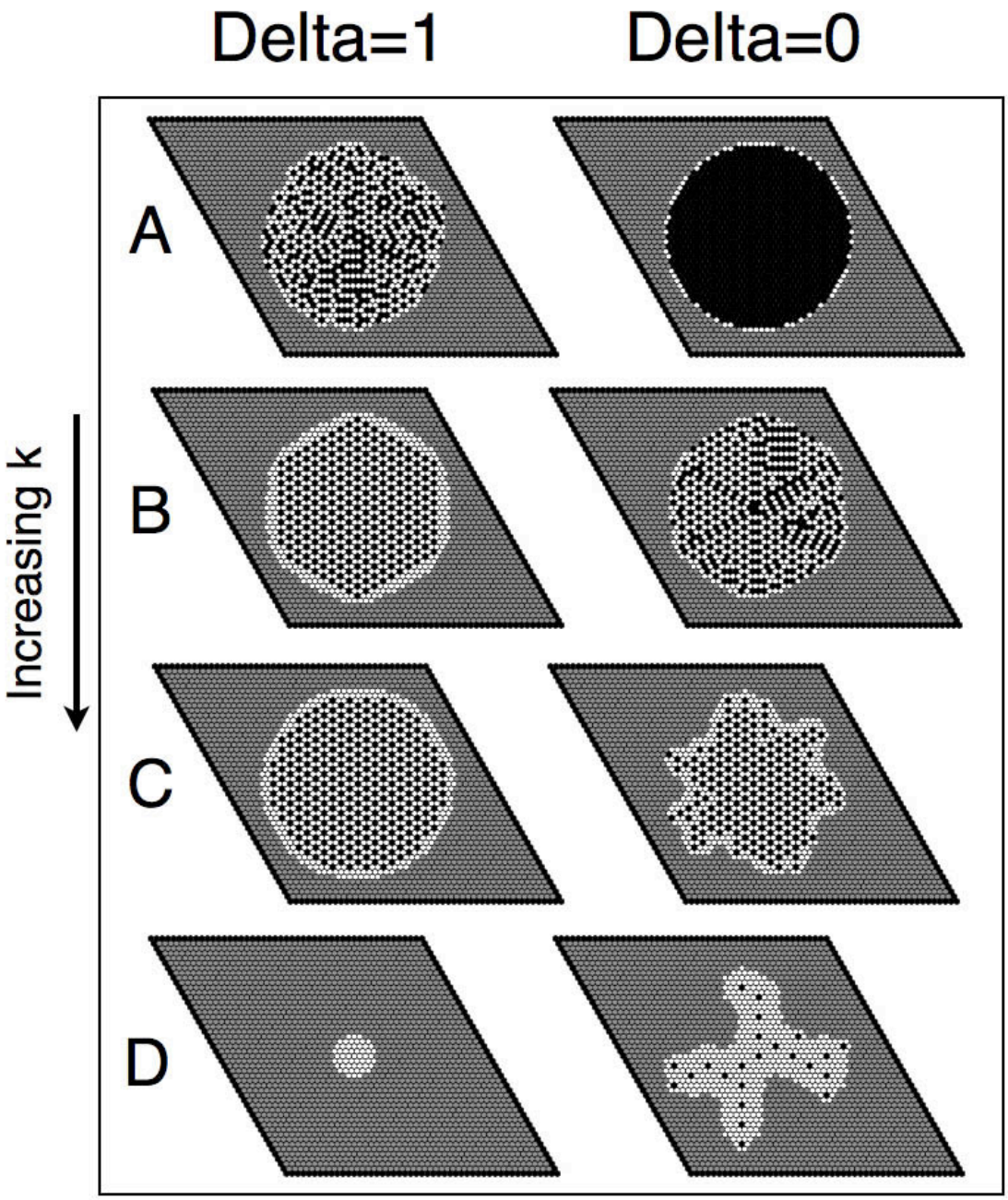

Fig. S5. Neurogenic patterns for hexagonal regular lattices display equivalent features to those on irregular lattices. (**A-D**) Snapshots of the stochastic neurogenic domain on a regular hexagonal lattice with a single central morphogen source for the parameter values indicated by circles (labelled A-D) inside the diagrams in supplementary material Fig. S4 for Delta=1 (left column) and Delta=0 (right column) conditions. (A) *k*=0.2511, (B) *k*=1, (C) *k*=10, (D) *k*=2511. In all cases, *b*=10,000. Front instabilities are clearly observed in the Delta=0 case and reflect the hexagonal

symmetry of the lattice. Note that this symmetry is only observed in regular lattices (compare with first row in Fig. S3). Grayscale code as in last row of supplementary material Fig. S1. Each snapshot corresponds to the final simulation time.

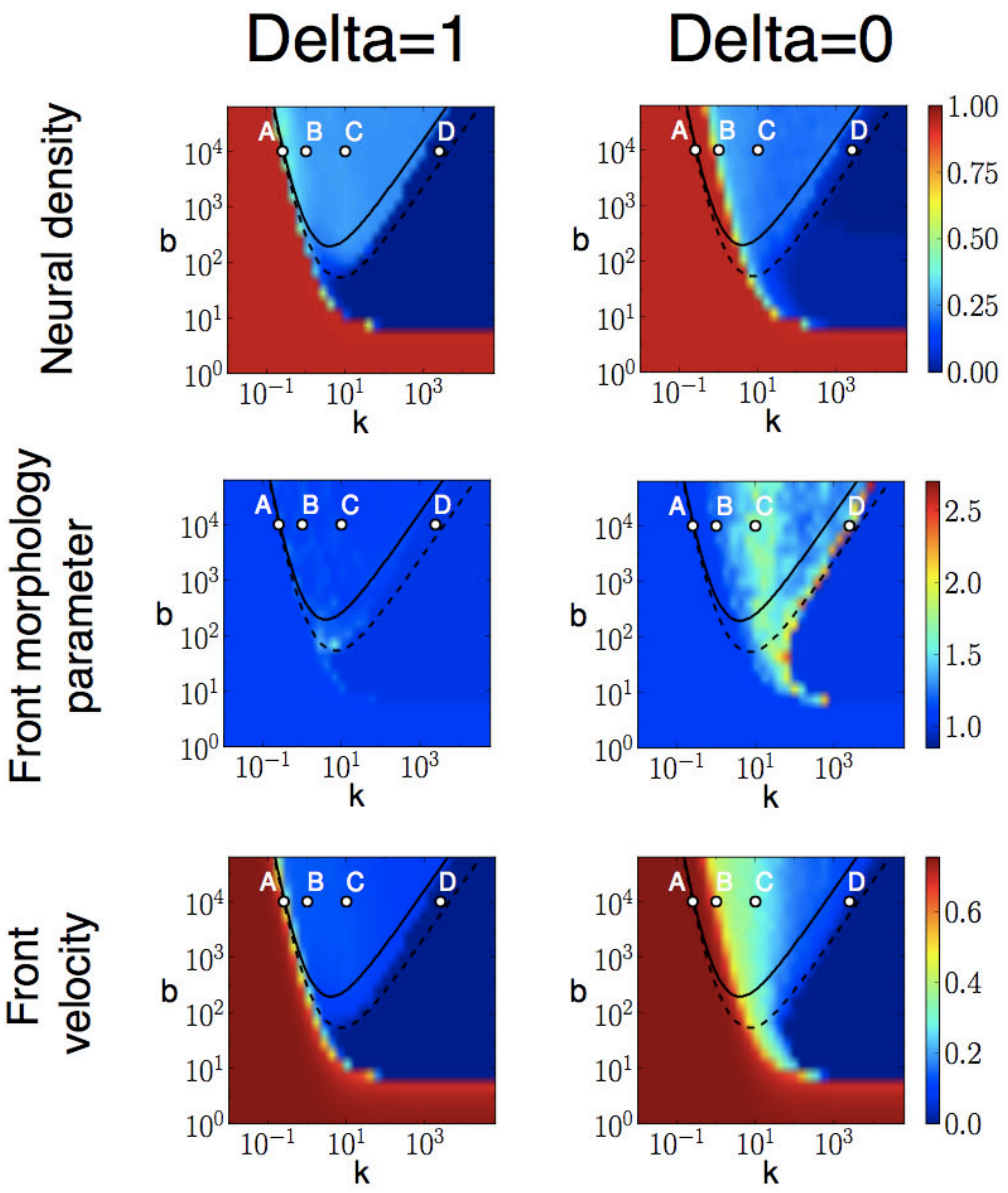

Fig. S6. Deterministic dynamics shows the same qualitative results as stochastic dynamics across the parameter space. Parameter space characterization of ρ (first row), Γ (second row) and v_f (third row) for Delta=1 (left column) and Delta=0 conditions (right column) as in Fig. 3 of the main text but for deterministic dynamics on an irregular lattice and with a single central morphogen source. Deterministic descriptions are appropriate for dynamics involving molecules with high copy number. Letters inside the diagrams denote different chosen representative points of the parameter space (see supplementary material Fig. S7). All remaining parameters and

conditions are as in Materials and methods in the main text. All deterministic simulations (supplementary material Figs S6-S13) were done with a Runge-Kutta algorithm of fourth order with time step dt=0.001.

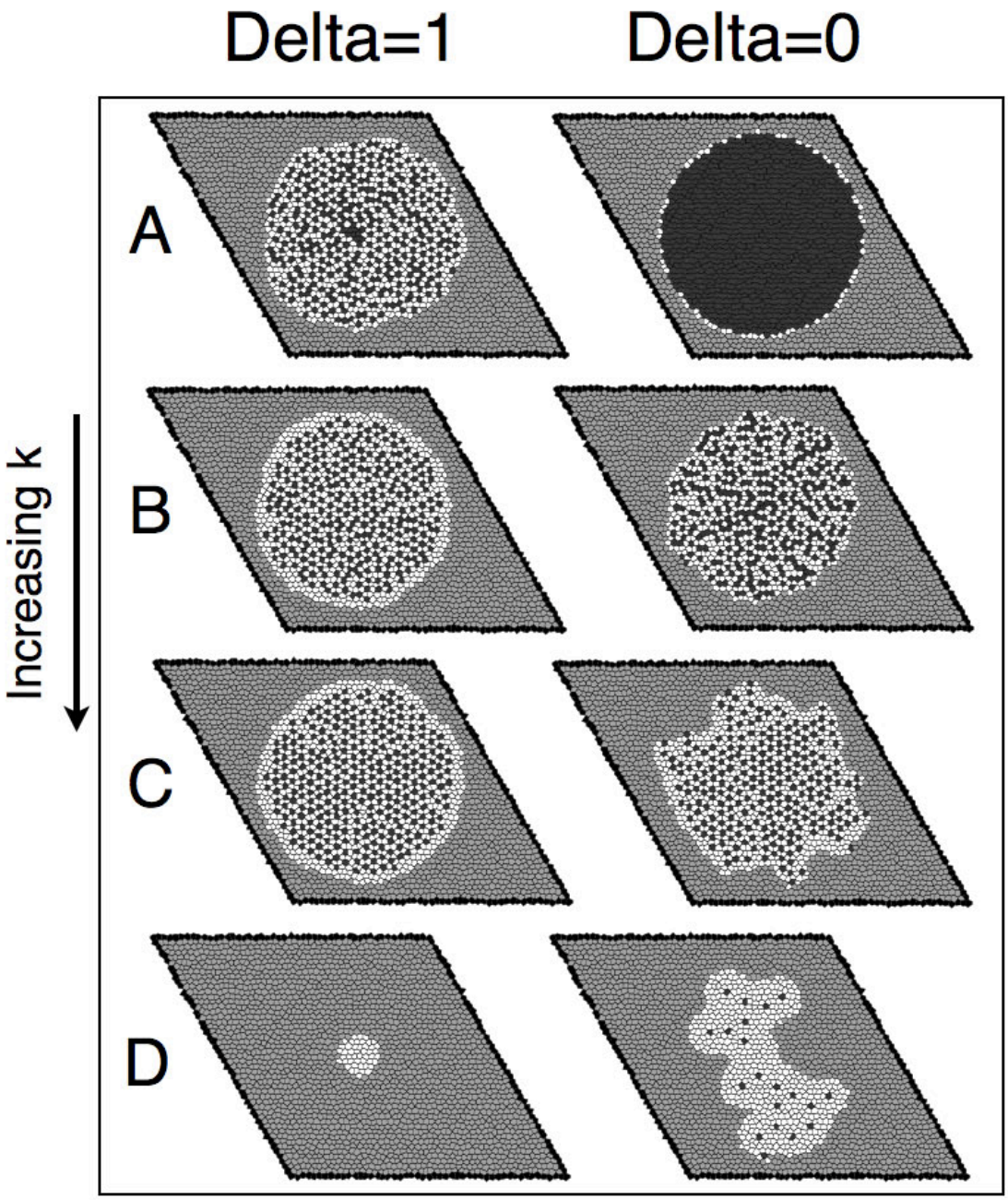

Fig. S7. Neurogenic patterns for deterministic dynamics are equivalent to those of stochastic dynamics. Snapshots of the deterministic neurogenic domain for the parameter values indicated by circles (labelled A-D) inside the diagrams in supplementary material Fig. S6 for Delta=1 (left column) and for Delta=0 (right column) conditions. (A) k=0.2511, (B) k=1, (C) k=10, (D) k=2511. In all cases, b=10,000. Deterministic (this figure) and stochastic snapshots (Fig. 4 in the main text)

are very similar. Grayscale code as in last row of supplementary material Fig. S1. Each snapshot corresponds to the final simulation time.

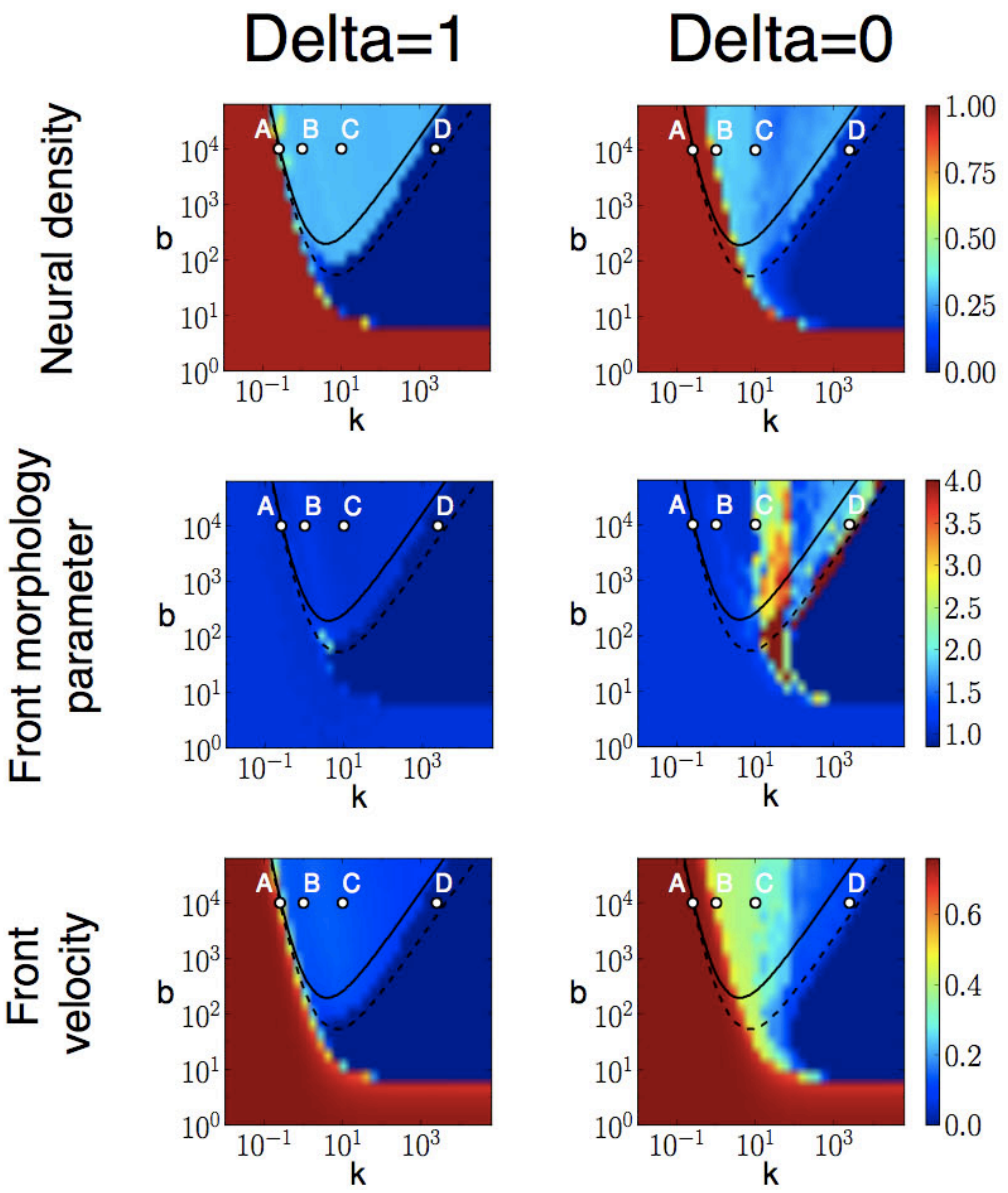

Fig. S8. Deterministic dynamics in hexagonal regular lattices show the same, but sharper, qualitative results. Parameter space characterization of ρ (first row), Γ (second row) and v_f (third row) for Delta=1 conditions (left column) and Delta=0 (right column) conditions as in Fig. 3 of the main text but for deterministic dynamics on a regular hexagonal lattice and with a single central morphogen source. For the Delta=0 case, $\Gamma>4$ values have been taken as $\Gamma=4$. Letters inside the diagrams denote different chosen representative points of the parameter space (see supplementary material Fig.

S9). All remaining parameters and conditions are as in Materials and methods in the main text.

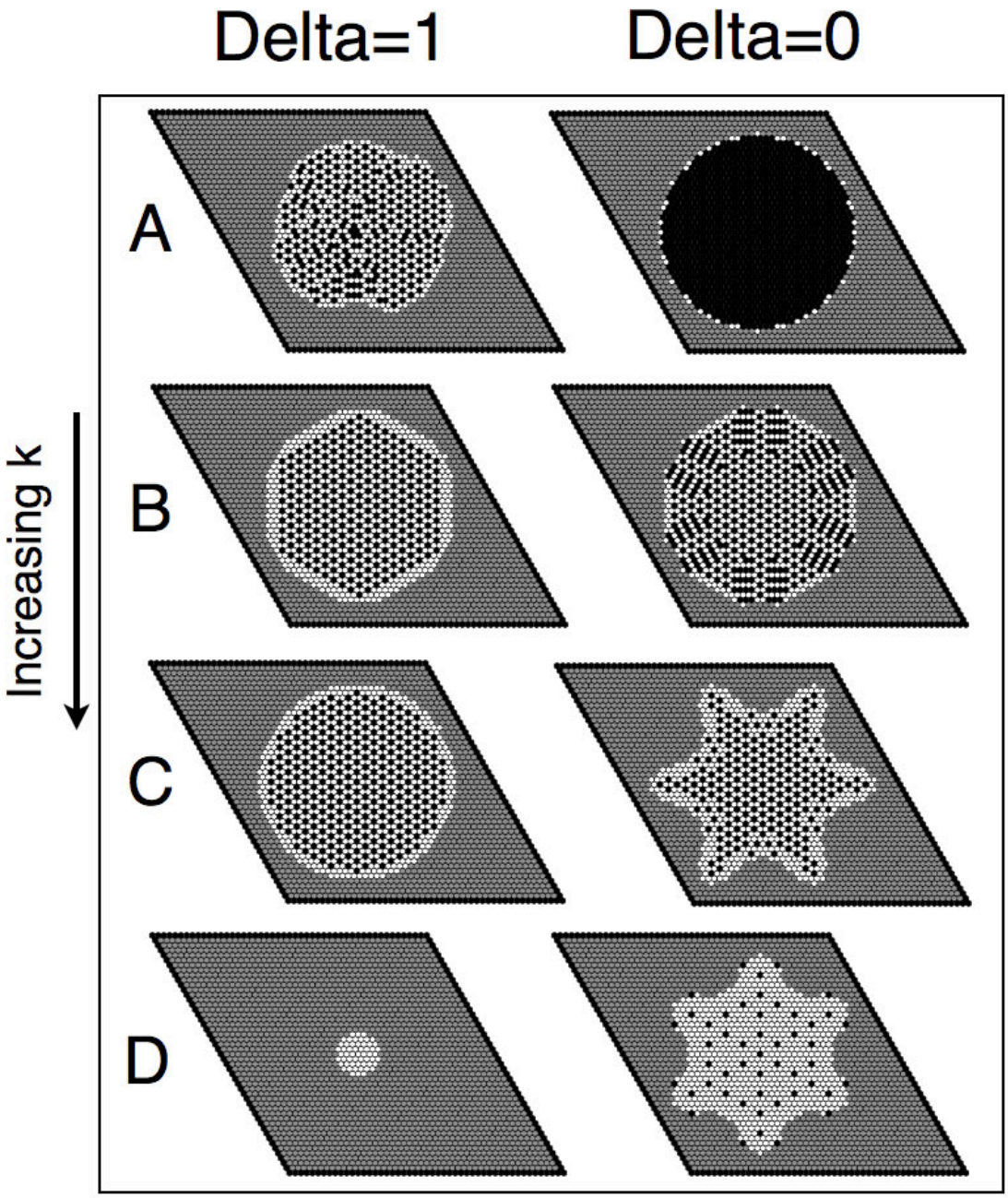

Fig. S9. Deterministic neurogenic patterns in hexagonal regular lattices display equivalent features to those of stochastic dynamics in irregular lattices. Snapshots of the deterministic neurogenic domain in a regular hexagonal lattice for the parameter values indicated by circles (labelled A-D) inside the diagrams in supplementary material Fig. S8 for Delta=1 (left column) for Delta=0 (right column) conditions. (A) k=0.2511, (B) k=1, (C) k=10, (D) k=2511. In all cases, b=10,000. Front instabilities are clearly observed in the Delta=0 case and reflect the hexagonal symmetry of the lattice.

Grayscale code as in last row of supplementary material Fig. S1. Each snapshot corresponds to the final simulation time.

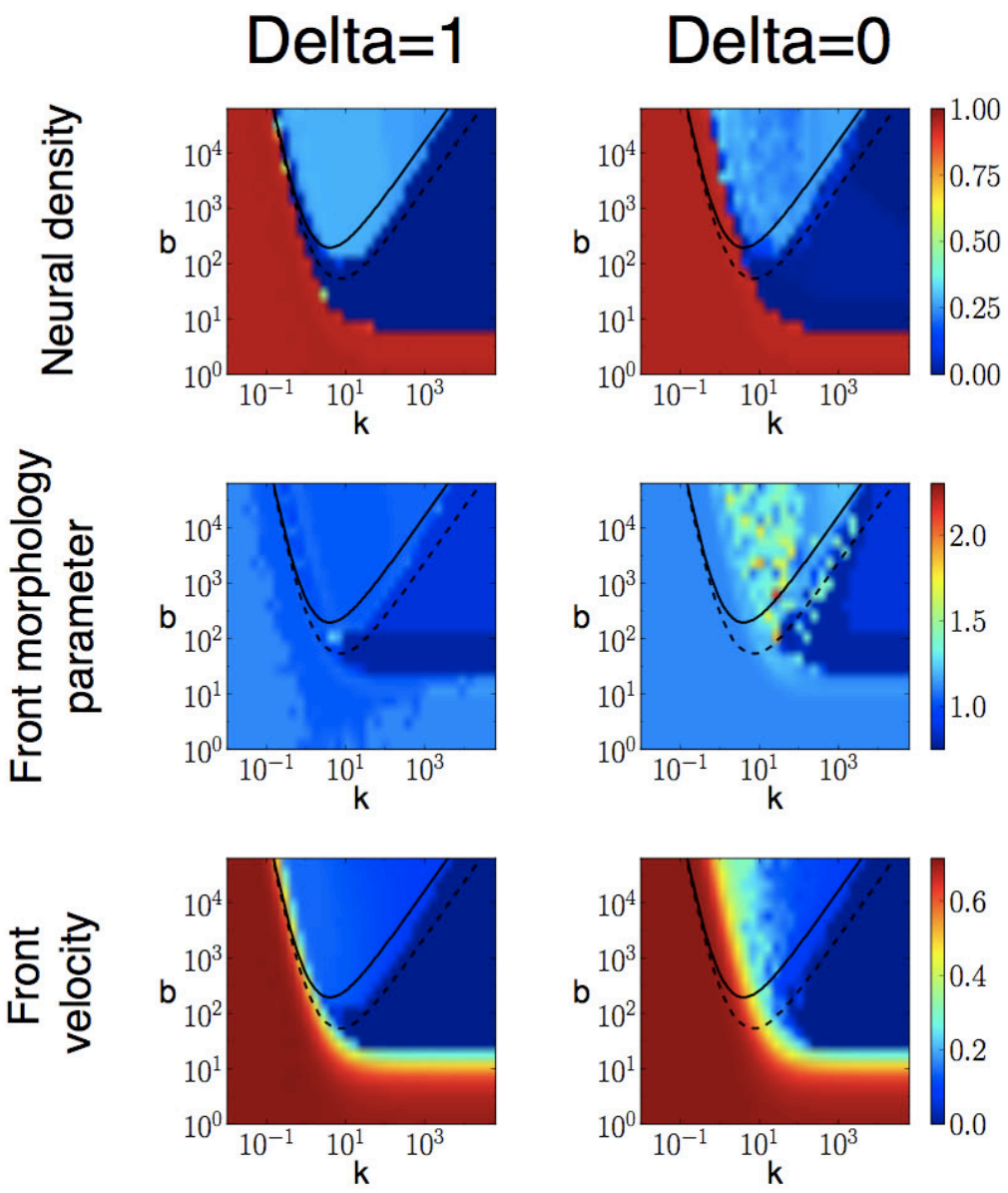

Fig. S10. Differentiable dynamics yield equivalent results. Parameter space characterization of ρ (first row), Γ (second row) and v_f (third row) for Delta=1 (left column) and Delta=0 (right column) conditions as in supplementary material Fig. S8 but for differentiable deterministic dynamics on a regular hexagonal lattice. The differentiable model reads:

$$\frac{dl_i}{dt} = v\left\{\frac{1}{1+bs_i^h} - l_i\right\}\Psi\left(m_i, m_c, q_m\right)\Psi\left(r_i, r_c, q_r\right)$$

$$\frac{ds_i}{dt} = \left\{\frac{k\langle l_i\rangle}{1+k\langle l_i\rangle} - s_i\right\}\Psi\left(m_i, m_c, q_m\right)\Psi\left(r_i, r_c, q_r\right)$$

$$\frac{dr_i}{dt} = v\left\{\frac{1}{1+bs_i^h} - r_i\right\}\Psi\left(m_i, m_c, q_m\right)\Psi\left(r_i, r_c, q_r\right)$$

$$\frac{dm_i}{dt} = u\left\{\Psi\left(r_i, r_c, q_{rm}\right) + D\Delta_i m_i - m_i\right\}$$

with $\Psi\left(x_i, x_c, q_x\right) = \frac{x_i^{q_x}}{x_c^{q_x} + x_i^{q_x}}$, q_m>0, q_{rm}>0 and q_r<0. Hill exponents have been set to $q_m = q_{rm} = -q_r = 10$. All remaining parameters and conditions are as in supplementary material Fig. S8. The qualitative results do not change with respect to the corresponding non-differentiable version of the model with step functions (supplementary material Fig. S8). Pattern snapshots are equivalent as well (data not shown).

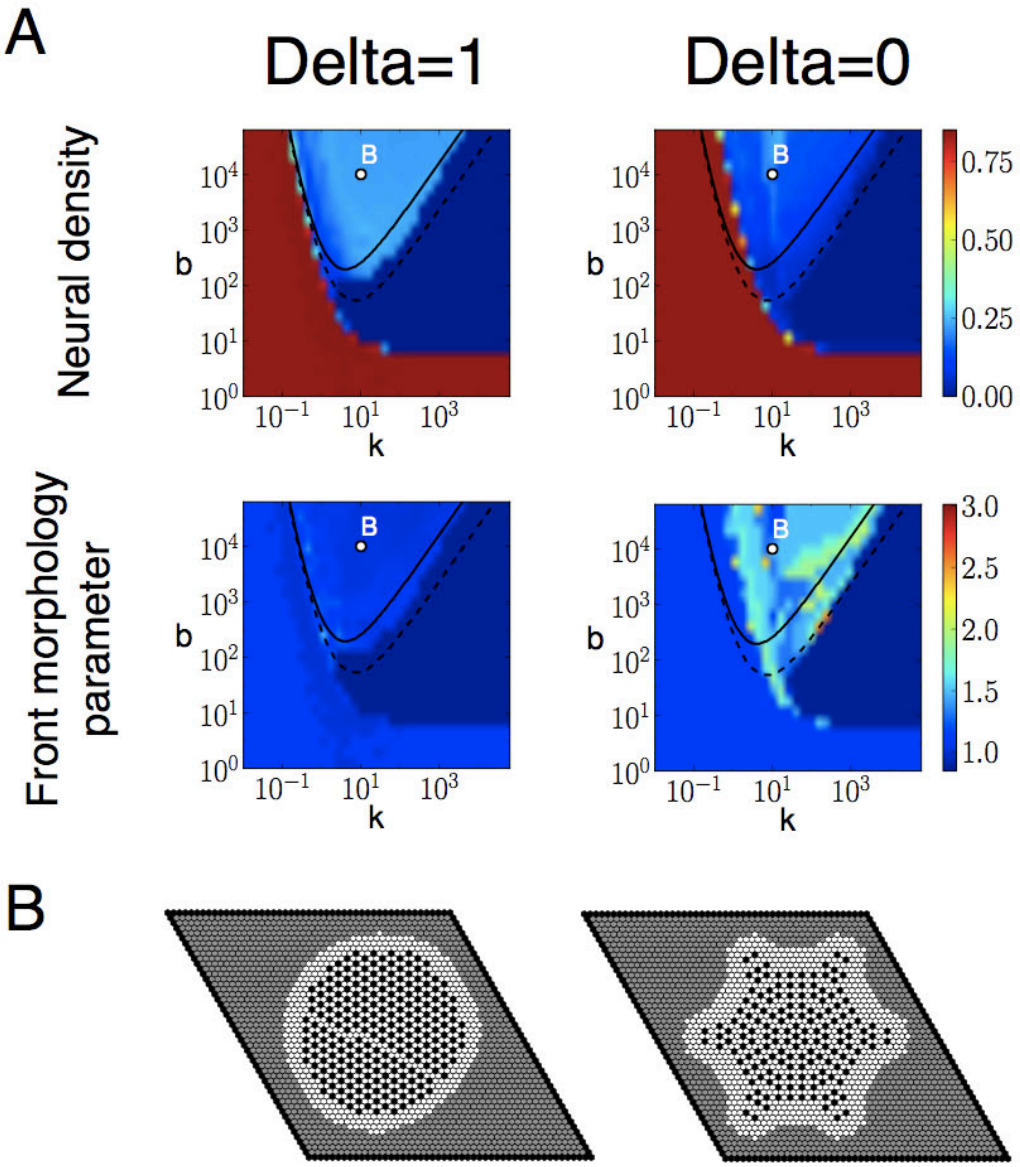

Fig. S11. Robust results for equivalent time scale dynamics of morphogen and signaling. (**A**) Parameter space characterization of ρ (first row) and Γ (second row) for Delta=1 (left column) and Delta=0 (right column) conditions for deterministic dynamics on a regular hexagonal lattice with u=1. (**B**) Patterns arising at the final time of simulation for the parameter values indicated by the letter B inside the diagrams in A (b=10,000 and k=10; grayscale code as in last row of supplementary material Fig. S1). All remaining parameters and conditions are as in supplementary material Fig. S8. The non-dimensional parameter u compares the time scale of the morphogen dynamics with

that of lateral inhibition signaling. The lower is *u*, the faster is the Notch signaling compared to the morphogen dynamics. *u*=1 corresponds to equivalent time scale dynamics of morphogen and signaling. Differences between the Delta=1 and the Delta=0 conditions for *u*=1 are similar to those for *u*=0.1 (supplementary material Figs S8 and S9).

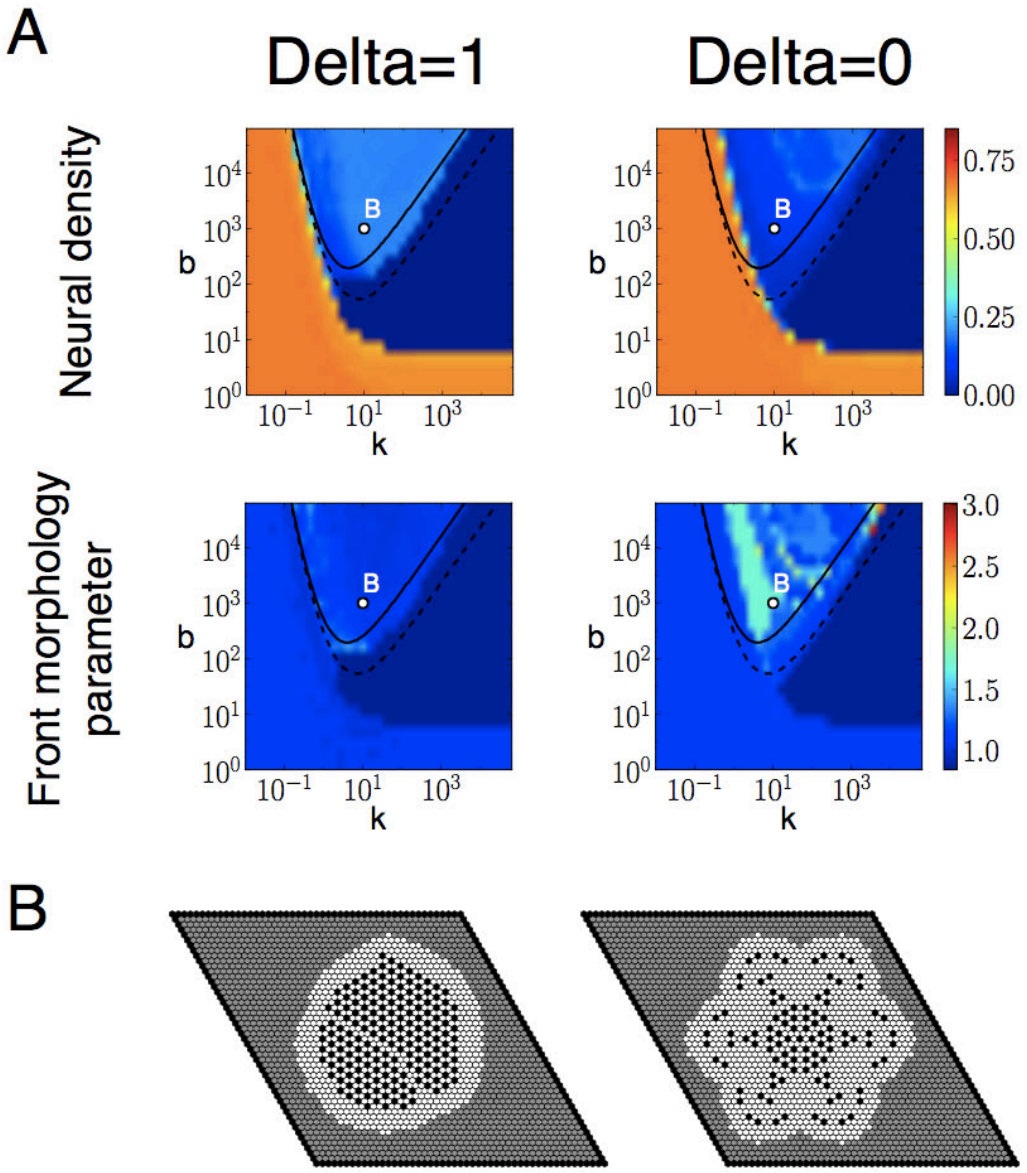

Fig. S12. Robust results for faster morphogen dynamics than signaling. (**A**) Parameter space characterization of ρ (first row) and Γ (second row) for Delta=1 (left column) and Delta=0 (right column) conditions for deterministic dynamics on a regular hexagonal lattice with u=10. u=10 corresponds to faster morphogen dynamics than signaling. (**B**) Patterns arising at the final time of simulation for the parameter values indicated by a letter B inside the diagrams in A (b=1000 and k=10; grayscale code as in last row of supplementary material Fig. S1). All remaining parameters and conditions are as in supplementary material Fig. S8. In the Delta=0 scenario, the front morphology

is less altered when the morphogen dynamics become so fast. Moreover, it exemplifies a situation where the pattern spreading is abnormal, and pattern initiation arises simultaneously in different regions of the tissue. In this figure, the faster Shh dynamics is also reflected in the wider border of cells having lateral inhibition dynamics but which have not yet differentiated. Differences between the Delta=1 and the Delta=0 conditions for u=10 are similar to those for u=0.1 (supplementary material Figs S8 and S9).

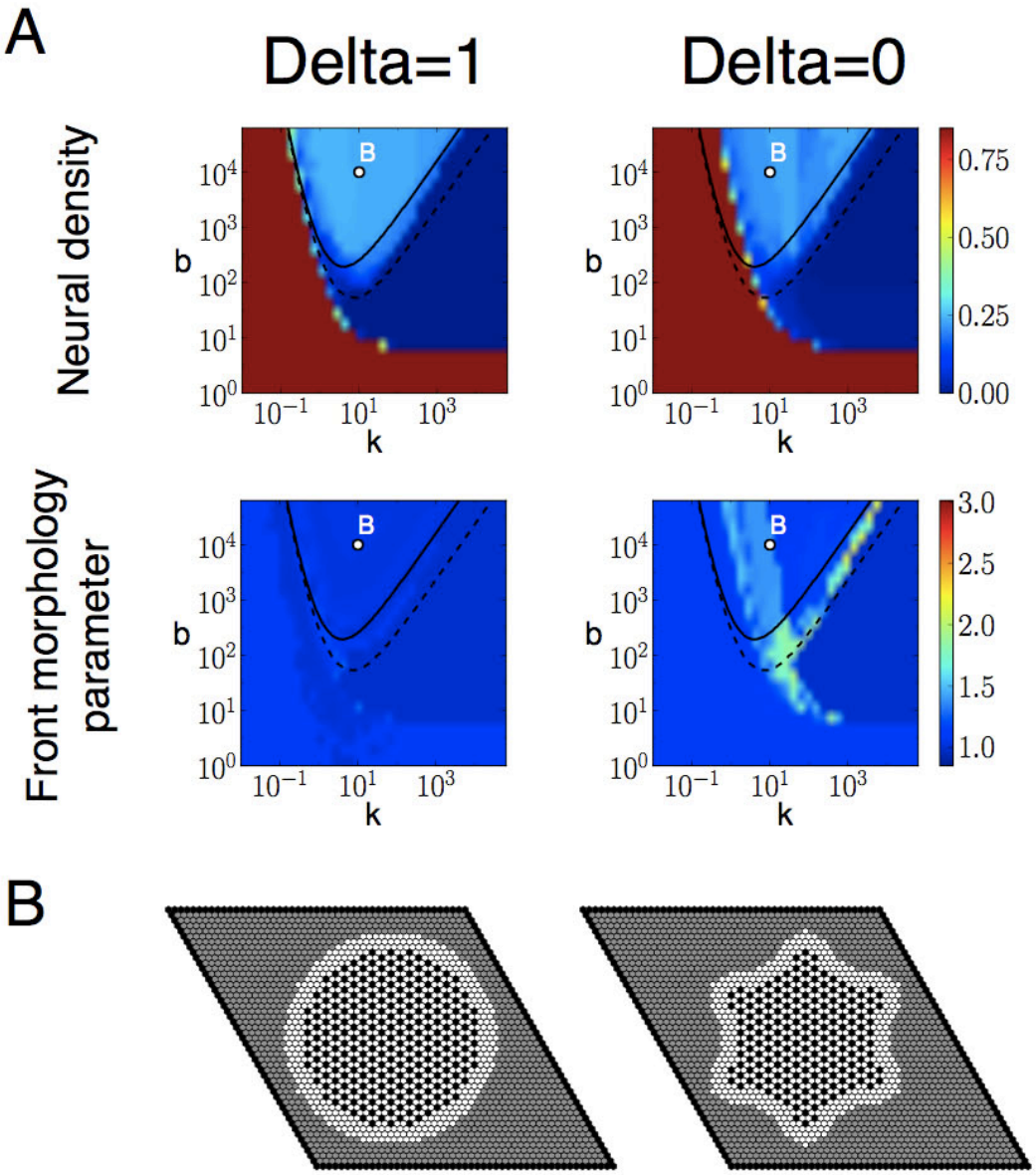

Fig. S13. Robust results for a longer-range morphogen. (**A**) Parameter space characterization of ρ (first row) and Γ (second row) for Delta=1 (left column) and Delta=0 (right column) conditions for deterministic dynamics on a regular hexagonal lattice with D=2.25. All remaining parameters and conditions are as in supplementary material Fig. S8. (**B**) Patterns arising at the final time of simulation for the parameter values indicated by a letter B inside the diagrams in A (b=10,000 and k=10; grayscale code as in last row of supplementary material Fig. S1). The non-dimensional parameter D controls the size of the initial neurogenic domain and the spatial range over which the

morphogen secreted by each source spans. Our numerical study indicated that a minimal value of D is required for pattern expansion, as it is necessary that the morphogen reaches new cells in order to start up their lateral inhibition dynamics. In this figure, the longer range of the morphogen is reflected in the wider border of cells having lateral inhibition dynamics but which have not yet differentiated. Results for D=2.25 are qualitatively similar to those for D=0.5625 (supplementary material Figs S8 and S9) with a reduced front morphological deformation across the parameter space. The value D=0.5625 corresponds to an effective range of morphogen influence of about two or three cells from the morphogen source cell. For large D values, abnormal situations arise in which pattern formation starts simultaneously in distant regions of the tissue (data not shown), which is enhanced when the morphogen dynamics is faster than the lateral inhibition dynamics (see supplementary material Fig. S12B). Therefore, the qualitative nature of our results holds for a finite range of morphogen spreading values, as expected. These values are consistent with the fact that the neurogenic pattern starts nucleating in a small patch of cells (Hu and Easter, 1999), and ensure that morphogen expression is not observed in front of the neurogenic wave, in agreement with experimental observations (Zhang and Yang, 2001; Neumann and Nuesslein-Volhard, 2000).